# PREDICTION OF PROTON AND NEUTRON ABSORBED-DOSE DISTRIBUTIONS IN PROTON BEAM RADIATION THERAPY USING MONTE CARLO N-PARTICLE TRANSPORT CODE (MCNPX)

A Thesis

by

BRIAN EDWARD MASSINGILL

Submitted to the Office of Graduate Studies of
Texas A&M University
in partial fulfillment of the requirements for the degree of

MASTER OF SCIENCE

August 2007

Major Subject: Health Physics

# PREDICTION OF PROTON AND NEUTRON ABSORBED-DOSE DISTRIBUTIONS IN PROTON BEAM RADIATION THERAPY USING MONTE CARLO N-PARTICLE TRANSPORT CODE (MCNPX)

A Thesis

by

BRIAN EDWARD MASSINGILL

Submitted to the Office of Graduate Studies of
Texas A&M University
in partial fulfillment of the requirements for the degree of

MASTER OF SCIENCE

Approved by:

| | |
|---|---|
| Chair of Committee, | John R. Ford |
| Committee Members, | John W. Poston, Sr. |
| | Michael Walker |
| Head of Department, | John W. Poston, Sr. |

August 2007

Major Subject: Health Physics

# ABSTRACT

Prediction of Proton and Neutron Absorbed-Dose Distributions in Proton Beam Radiation Therapy Using Monte Carlo N-Particle Transport Code (MCNPX). (August 2007)

Brian Edward Massingill, B.S., Texas A&M University

Chair of Advisory Committee: Dr. John R. Ford

The objective of this research was to develop a complex MCNPX model of the human head to predict absorbed dose distributions during proton therapy of ocular tumors. Absorbed dose distributions using the complex geometry were compared to a simple MCNPX model of the human eye developed by Oertli. The proton therapy beam used at Laboratori Nazionali del Sud-INFN was chosen for comparison. Dose calculations included dose due to proton and secondary interactions, multiple coulombic energy scattering, elastic and inelastic scattering, and non-elastic nuclear reactions. Benchmarking MCNPX was accomplished using the proton simulations outlined by Oertli. Once MCNPX was properly benchmarked, the proton beam and MCNPX models were combined to predict dose distributions for three treatment scenarios. First, an ideal treatment scenario was modeled where the dose was maximized to the tumor volume and minimized elsewhere. The second situation, a worst case scenario, mimicked a patient starring directly into the treatment beam during therapy. During the third simulation, the treatment beam was aimed into the bone surrounding the eye socket to estimate the dose to the vital regions of the eye due to scattering. Dose distributions observed for all three cases were as expected. Superior dose distributions were observed with the complex

geometry for all tissues of the phantom and the tumor volume. This study concluded that complex MCNPX geometries, although initially difficult to implement, produced superior dose distributions when compared to simple models.

*This work is dedicated to several individuals who, if not for them, I would not be where I am today.*

*To Jesus – Thank you for guiding me true and giving me the courage and strength to persevere through all life's challenges.*

*To Punkin & Memaw, Robert B. and Tommie J. Massingill – Thank you for always being there and pushing me to do my best. Without your love and support, I would not be the person that I am today.*

*To Granny, Gracie L. Flory – Thank you for being such a strong individual and showing me that when life knocks you down, God is always there to pick you up. Rest in Peace.*

*To Mom and T.J. (Dad), Margaret J. and Thurman Moore, Jr. – Thank you for raising me to know God and for the courage to pursue a life filled with success and happiness.*

*To Dad, Robert D. Massingill, Sr. – Thank you for the advice, guidance and encouraging words when I was confused as to which path to take.*

*To my brother, Robert D. Massingill, Jr., – Thank you for setting the example of what a successful individual should be. I am very lucky to have you as a big brother.*

*To my girlfriend, Tamara L. Gill – Thank you for standing by my side throughout the trials and tribulations of my college career.*

*To my brothers, Brandon D. Moore and Dalton L. Massingill – Thank you for allowing me to set the example for you just as Robert has set the example for me. Never forget, "Anything worth having is worth working for." – John Burroughs*

*You have all provided me with endless love and support and are all a constant catalyst for growth and an inspiration in love.*

*I love you all.*

## ACKNOWLEDGEMENTS

I would like to thank my advisor and committee chair, Dr. John R. Ford, for his patience, guidance, and unwavering support during this research. I would also like to thank my committee member, Dr. John W. Poston, Sr., for answering my many questions, his guidance during both my undergraduate and graduate careers, and his keen eye for editing. Additionally, I would like to thank my committee member, Dr. Michael Walker, for his support in all my efforts during this research.

# TABLE OF CONTENTS

Page

Page

# LIST OF FIGURES

FIGURE Page

FIGURE Page

# LIST OF TABLES

# CHAPTER I

# INTRODUCTION AND BACKGROUND

*Proton vs. Conventional Radiotherapy*

The goal of conventional radiation therapy is to deliver radiation to a target volume within the human body while sparing the surrounding normal tissues. Intensity-modulated radiation therapy (IMRT), the most advanced method for photon delivery, helps to minimize the dose to healthy tissues by applying radiation fields of varying intensities and directions to the target tissue. However, because the photon does not have complete energy deposition within the tumor volume, residual dose is delivered to normal tissues along the path of the photon beam; thus resulting in a large planning treatment volume (PVT) and a large integral dose. A constant concern associated with IMRT is the growth of secondary malignancies due to radiation-induced damage to the DNA of surrounding healthy tissues.

In comparison, protons irradiate a smaller volume of normal tissue at higher doses than is feasible with IMRT. This is due to the differences between photon and proton energy deposition characteristics. Photon energy decreases exponentially with depth in a material while protons have a finite range with no residual dose beyond that point. As with all charged particles, protons have a rapid energy loss near the end of their track, which causes a large peak in the deposited dose, known as the Bragg peak. The depth at which the Bragg peak occurs is directly related to the initial energy of the incident protons. Hence the Bragg peak, i.e. the region of maximum dose, can be precisely placed

---

This thesis follows the style of the journal of Health Physics.

within the tumor volume. For irradiation purposes, both the intensity and energy of the incident proton is varied to achieve the desired dose within the tumor volume. Modulation of the proton beam results in a spread out Bragg peak (SOBP) that delivers a uniform dose across the malignant volume. "[Therefore], in contrast to photon radiotherapy, a single proton field can achieve dose conformation to the target volume" (Levin et al. 2005). A depth-dose comparison of a 15-MV potential photon beam and a SOBP is shown in Fig. 1. Here, the SOBP has been developed to provide a high, uniform dose within the tumor volume (Smith 2006).

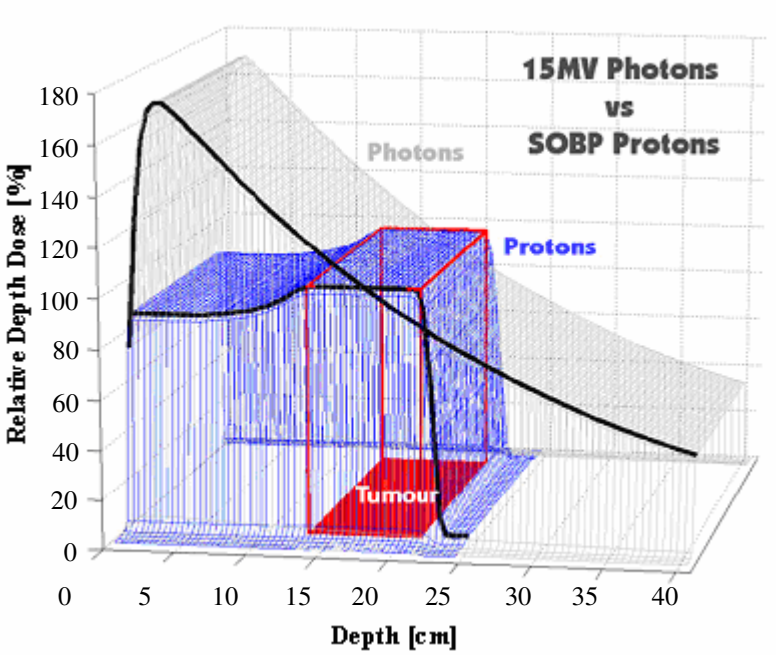


**Fig. 1:** Dose/depth comparison of 15-MV photons and intensity-modulated protons (Smith 2006)

Due to its energy deposition characteristics, proton radiotherapy is replacing many tumor treatment methods. One example is enucleation of the eye resulting from malignant melanoma. Although radiation therapy can damage critical organs of the eye

necessary for eyesight, radiotherapy is considered a conservative method of treatment when comparing alternatives.

*Objective*

The objective of this research was to perform a comparison between two MCNPX models of the human eye that approximate doses delivered during proton therapy. Oertli's (2006) simple MCNPX model of the human eye will be compared to a complex MCNPX geometry that incorporates the entire human head. Calculations using these models will provide approximate doses delivered during proton therapy due to proton interactions, "secondary interactions including multiple columbic energy scattering, elastic and inelastic scattering, and non-elastic nuclear reactions (i.e., the production of secondary particles)" (Oertli 2006). In addition, proton and neutron absorbed-dose distributions throughout the human head will be obtained using the complex MCNPX model. The steps to completion included:

1. Selection of the proton beam to model.
2. Benchmarking MCNPX using a simple phantom simulation to ensure proper functioning of the code during proton attenuation/dose depth calculations.
3. Constructing the complex geometry of the human head.
4. Incorporating the selected proton beam with eye models.
5. Incorporate the geometry, the eye models and the proton beam into the computer code.
6. Simulation of proton-radiation therapy treatments using an appropriate number of proton histories.

7. Observe comparison of the dose distributions found with models.
8. Observe dose distributions throughout the human head model.

*Status of the Question and Model Development*

As early as 1946, Wilson proposed the potential application of protons and other charged particles in radiation therapy (Raju 1980). Since that time great strides have been made to tap this potential and make proton radiotherapy a reality. As early as the 1950's, patients with pituitary tumors were being treated (Gargoundas 2006). Since that time, more than 30,000 patients world wide have been treated at more than 20 research facilities. Most proton radiotherapy treatments have been concentrated on small sites in the skull and head-and-neck region, with Constable and Koehler being the first to identify the benefits of proton treatment in ocular tumors. In 1975, the first eye melanoma was treated (Turesson et al. 2003; Constable and Koehler 1974; Gargoundas 2006). In the mid to late 1970s, preclinical studies of proton therapy were being conducted to assess the efficiency of proton beams on intraocular tumors. Lesions were being induced on the fundus of monkey eyes and irradiate with collimated beams to demonstrate the efficiency and selectivity of proton radiotherapy (Gargoundas 2006). Further research, conducted after proton radiotherapy was established as a means to treat ocular melanoma, improved the accuracy with which proton radiotherapy could be delivered. In the early 1980s a comparison of the survivability of patients who had undergone radiotherapy to those who had undergone enucleation was made to further substantiate protons as a treatment modality (Gargoundas 2006). A comparison of ocular melanoma pre-irradiation and post-irradiation is shown in Fig. 2.

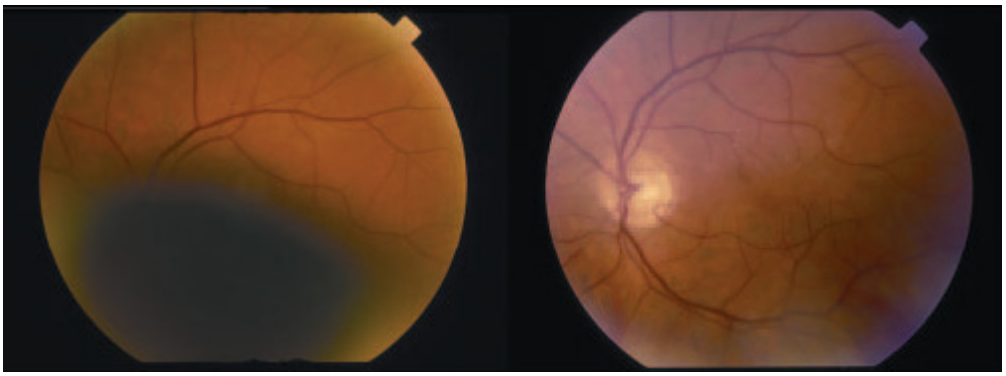

**Fig. 2**: A tumor covering the optic disc and macula before proton radiation (visual acuity of 20/100 (*left*)) and thirty-eight months after proton therapy (tumor regression and visual acuity of 20/25 (*right*)) (Gargoundas 2006)

The Monte Carlo method has been used for centuries; however, only in the past several decades has the method gained the status of a numerical method capable of addressing the most complex applications. In 1986, two-dimensional Monte Carlo codes were pioneered. These codes were used to study factors that influenced the edge of the proton beam at the Harvard Cyclotron. Here, research was conducted to determine the efficiency and effectiveness of various collimating apertures and range compensators of the proton beam (Urie et al. 1986). In 1995, a milestone was reached in proton radiotherapy research. Monte Carlo simulations were combined with proton imaging to increase precision during alignment of the patient and proton beam (Romero 1995). Due to early concerns about the radioresistance of ocular melanomas and precision of proton radiotherapy, the mortality rate of 2069 patients was carefully monitored. To date, the five-, 10-, and 15- year survival rates are 86%, 77%, and 73%, respectively (Gargoundas 2006). These rates are comparable to five-year survival rates using modern proton facilities (Gargoundas 2006). In 1998 secondary radiation doses initiated by proton

therapy, fluence rates and the relative biological effectiveness of protons in ocular treatments were studied using Monte Carlo simulations (Agosteo et al. 1998; Paganetti 1998). In 2000, two Monte Carlo codes were benchmarked—the Los Alamos High Energy Transport Code (LAHET) and the Monte Carlo N-Particle Transport Code (MCNPX) against a proton radiotherapy beam utilized at Loma Linda University Medical Center. Both codes simulated the patient-specific dose distributions for proton radiotherapy in prostate cancer (Oertli 2006). The development of MCNPX was a major undertaking at Los Alamos National Laboratory (LANL) for several years (Hughes et al. 2000). Through the efforts of researchers, MCNPX has become the cornerstone for many particle transport applications including protons. In 2001, a systematic Monte Carlo study was conducted on secondary electron fluence perturbation in clinical proton beams. Using Monte Carlo algorithms, beams from 70–250 MeV were modeled to assess perturbation effects from cavity ion chambers to increase the effectiveness of proton radiotherapy (Verhaegen and Palmans 2001). In 2004 GEANT4, a Monte Carlo algorithm, was applied to a CT-voxel benchmarking the phantom in a manner similar to Siebers in 2000 (Paganetti et al. 2004). The Midwest Proton Radiotherapy Institute in Bloomington, Indiana began operations in 2004 and, by the end of last year, the Shands Medical Center in Jacksonville, Florida and the M.D. Anderson Cancer Center in Houston, Texas began seeing patients to treat eye tumors and other malignancies with extensive modeling of their respective beam being completed in MCNPX (Gargoundas 2006).

In principle, the Monte Carlo transport technique can provide accurate predictions of the proton treatment beams used in today's proton treatment facilities. To date, Monte

Carlo transport codes can take into account all physical processes involved in proton treatment. Coulombic energy loss, energy straggling, multiple Coulomb scattering, elastic and non-elastic nuclear interactions, and the transport of secondary particles can be simulated and resolved in a reasonable time frame (Oertli 2006). It has not been shown, however, whether it is possible to commission a proton treatment facility using data obtained by Monte Carlo predictions alone (Newhauser et al. 2005).

# CHAPTER II

# THE MODEL

*Benchmarking*

Benchmarking the MCNPX computer code was accomplished using the same method outlined by Oertli (2006). A 10-cm diameter, 200-MeV proton beam entering a 10-cm radius, 30-cm high (vertical z-axis) cylinder phantom was constructed. For qualitative purposes, three small cylinders (normal to the z-axis) were modeled at different locations within the phantom and assigned a proton importance. One cylinder was defined as a zero importance region, i.e., any proton entering its volume would cease to exist. The second and third cylinders were defined as having an importance of one; however, one cylinder was defined as iron and the other as being void. For qualitative purposes, a heating mesh tally was used to demonstrate the interactions (or lack thereof) that occured within the three cylinders. The results are shown in Fig. 3. Here the blue and red color schemes indicate cool and hot regions, respectively.

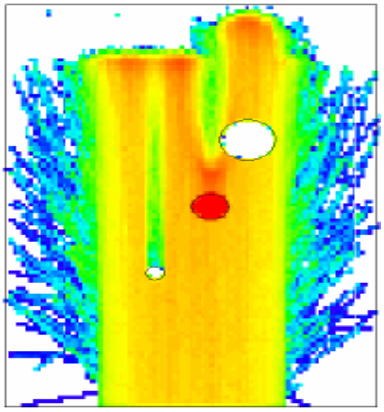

**Fig. 3**: Heating mesh tally of 200-MeV protons entering a water phantom. Cylinders (from left to right) (a) zero importance, (b) iron, (c) void

As expected, the proton beam was "killed" within the zero importance region (left) resulting in limited reactions within the volume (not all particles were assigned zero importance) and a shadow cast down stream from the proton source. The shadow is a consequence of the sudden cooling due to the decrease in the number of protons and thus interactions above the zero importance region. As anticipated, the iron cylinder (center) was the hottest region within the phantom. The higher density of the iron resulted in a high interaction rate, a shorter proton range after the cylinder and greater heating within and following the iron. The void cylinder (right) provided expected results also. No interactions were recorded within the volume thus resulting in a longer proton range following the void. All three cylinders yielded expected results confirming that the MCNPX code was, quantitatively, performing as expected.

Benchmarking the code for radiotherapy purposes was accomplished using the 62-MeV proton beam from the Laboratori Nazionali del Sud-INFN for two different scenarios. First, the source energy and beam diameter of the model were adjusted to match the 62-MeV beam and the three cylinders were removed. The original phantom was subdivided into progressive layers and deposited energy was tallied within each layer of water; thus measuring energy deposition as a function of depth in the phantom. As expected, the energy deposition curve showed the characteristic Bragg peak; however, the maximum energy deposition occurred at a greater depth in the phantom. The variation in maximum penetration depth is due to electron straggling effects and the low energy cut-off in MCNPX simulations. The MCNPX code cannot be used to track protons and scattered electrons with energies lower than 1 keV and 1 MeV, respectively. This limitation means that the dose deposited by both delta rays and low-energy

protons (< 1MeV) is neglected; thus explaining the difference between the two curves. A comparison between the simulated and measured values in a water phantom is shown in Fig. 4.

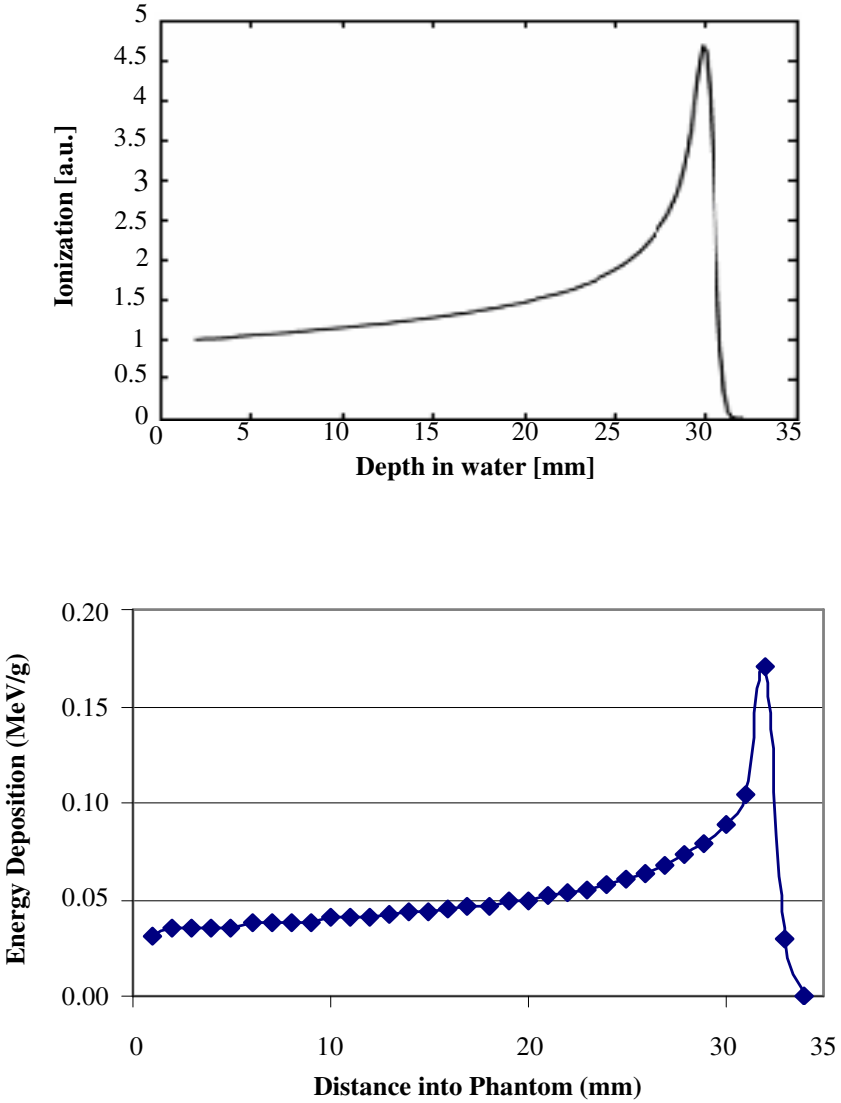


**Fig. 4**: Measured ionization (top) (Cirrone et al. 2004), MCNPX energy deposition (bottom) as a function of depth into water and the phantom, respectively

Secondly, the actual data collected at the Laboratori Nazionali del Sud-INFN were simulated. In practice, a modulator is frequently incorporated into the treatment

scenario to vary the beam energy and thus the range of the protons exiting the modulator. Using a modulator wheel with varied material characteristics effectively and efficiently generates a proton-energy spectrum that produces a uniform dose distribution over a target volume. The resulting energy deposition curve is illustrated in Fig. 5 and is called a spread out Bragg peak (SOBP). This curve is obtained by summing the individual Bragg peaks created by the various proton energies. The resulting proton beam uniformly deposits a higher dose in the target volume.

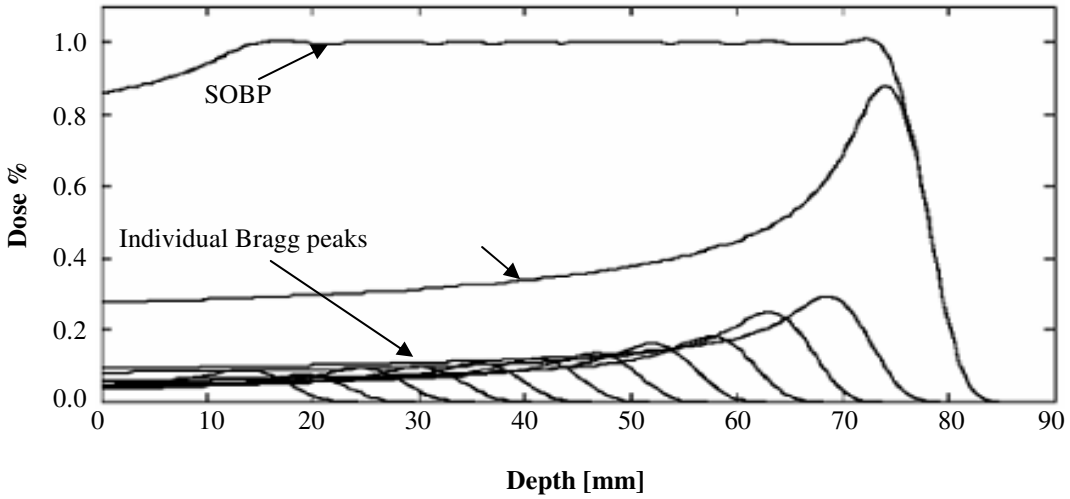


**Fig. 5**: SOBP resulting from the sum of individual Bragg peaks (Kooy 2003)

Using the proton energy spectrum and frequency with which each energy should be introduced into the beam as determined by Oertli (2006), the characteristic SOBP resulting from the proton beam at the Laboratori Nazionali del Sud-INFN was generated. The resulting Bragg peak, shown in Fig. 6, closely resembled actual data. Slight variations between the two curves are a result of the limited ability to use the MCNPX code to track low energy electrons (<1 keV) and low energy (< 1MeV) protons, as

previously discussed. However, with these results the MCNPX code was appropriately benchmarked.

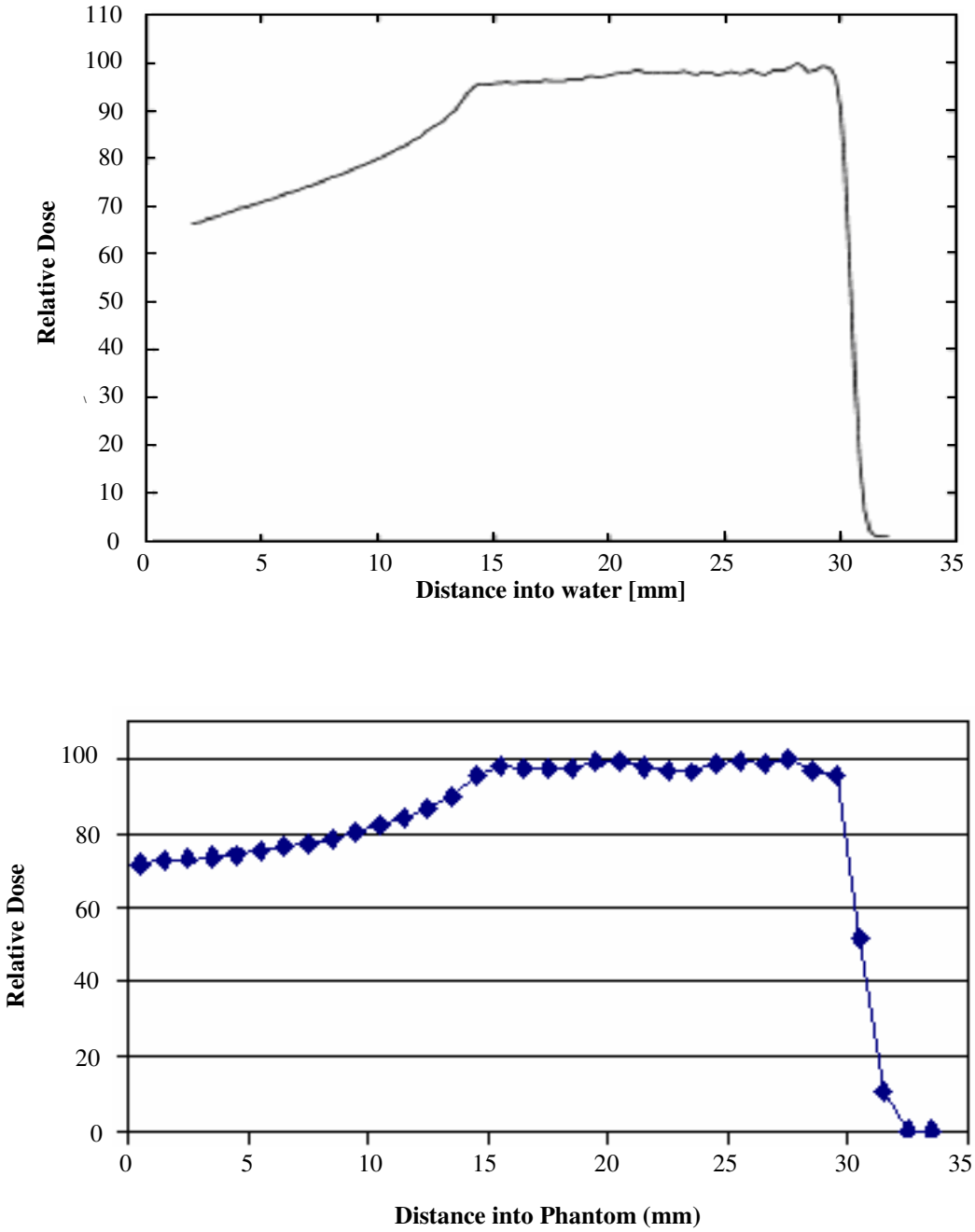


**Fig. 6**: Measured SOBP (left), simulated SOBP (right) (Cirrone et al. 2004)

*The Phantom*

Although the focus of the model to be used in the dose calculations was placed on critical structures of the eye such as the lens, cornea, optic nerve, choroid and sclera, all structures of the human head including but not limited to the brain, cerebral fluid, temporal lobe, spinal cord, and sinuses were of concern. For that reason, a complex geometry was chosen for all simulations performed.

The Zubal head phantom, a voxel-based anthropomorphic phantom created by Zubal (2007), is a phantom of the human head created by segmenting MRI head slices of two living human males. The manually segmented 124 transverse MRI slices were used to create a computerized 3-dimensional volume array; thus modeling all major internal structures of the human head (Zubal 2007). The transverse slices were recorded in a 256 x 256 matrix having isotropic voxel dimensions of 1.5 mm. Originally, the phantom contained sixty-two neurological and taxonomical structures in the human brain as well as anatomical regions and was contained within a 256 x 256 x 128 byte array (Zubal 2007). A cross-section of the original Zubal head phantom is shown in Fig. 7. Here critical structures of the eye including the lens and optic nerve, in addition to critical structures of the brain including the cerebellum and temporal lobe, are visible.

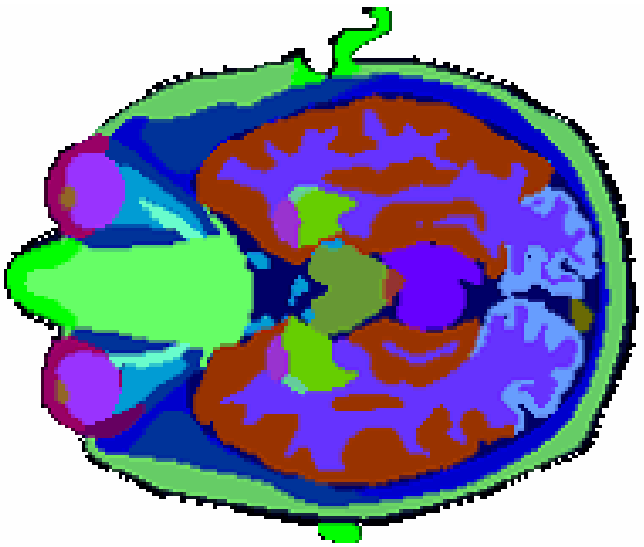

**Fig. 7**: Cross section of the original Zubal head phantom as viewed from above (Zubal 2007)

For the purposes of the simulations conducted, a modified Zubal head phantom was used. The modified phantom, which models 29 critical structures of the human head, was created by Jeff Evans with revisions by Chenguan Li at the Department of Mechanical Engineering at The Ohio State University (Evans and Li 2007) and is based on the original Zubal phantom. Most of the modified head geometry is 85 x 109 x 120 lattice of voxels, where each voxel is 2.2 x 2.2 x 1.4 $mm^3$ (Evans and Li 2007). To obtain a cross-sectional representation of the modified Zubal phantom a MATLAB routine (Appendix A), developed by Pasciak (2007), was used. The routine was used to read the original voxel map into a three-dimensional matrix, which allowed cross-sections of the phantom to be plotted and modifications made. Fig. 8 is a voxel cross-section of the modified Zubal head phantom. Again the critical structures of the eye and brain are illustrated. Volumes and material compositions of all structures included in the modified Zubal phantom were calculated and included in the original MCNPX input deck prepared by Evans and Li (2007).

Further modifications to the modified Zubal head phantom were necessary to complete the required simulations. First, a large (stage 3) 3 x 7 x 4 voxel tumor with a volume of 81.2 $mm^3$ was inserted into the phantom located in the upper right quadrant of the right eye. Each voxel of the tumor was defined as an independent region in which absorbed dose was calculated.

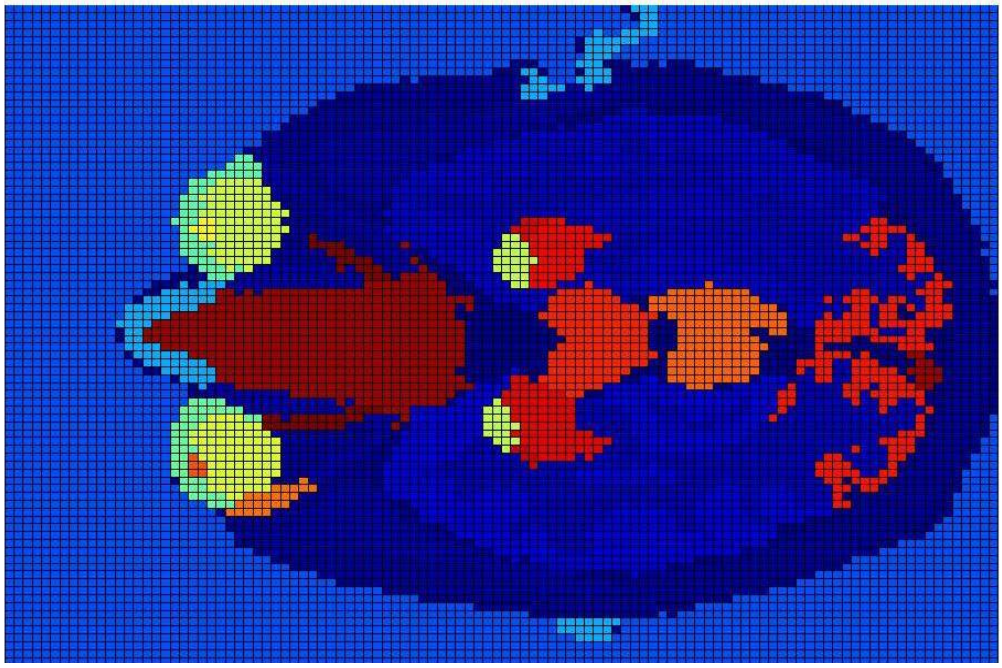

**Fig. 8**: Cross section of the modified Zubal head phantom

Defining each voxel independently of one another produced a dose distribution across all regions of the lesion. Cirrone et al. (2004) reported that the majority of the patients examined in a study conducted at the Laboratori Nazionali del Sud-INFN suffered from stage T3 uveal melanomas (large lesions); therefore, a large lesion was chosen. As shown in Table 1, among the uveal melanomas treated, 28 patients were stage T3 (60%), 17 stage T2 (36%) and 2 stage T1 (4%) (Cirrone et al. 2004).

It was also important to determine a dose deposition to healthy tissues surrounding the tumor. This was accomplished by defining and calculating the dose deposition within a series of voxels surrounding the tumor. These voxels were defined as being independent of surrounding tissues while maintaining their respective material properties. Cross sections of each layer of the tumor indicating voxel numbers and surrounding tissues are shown in Fig. 9.

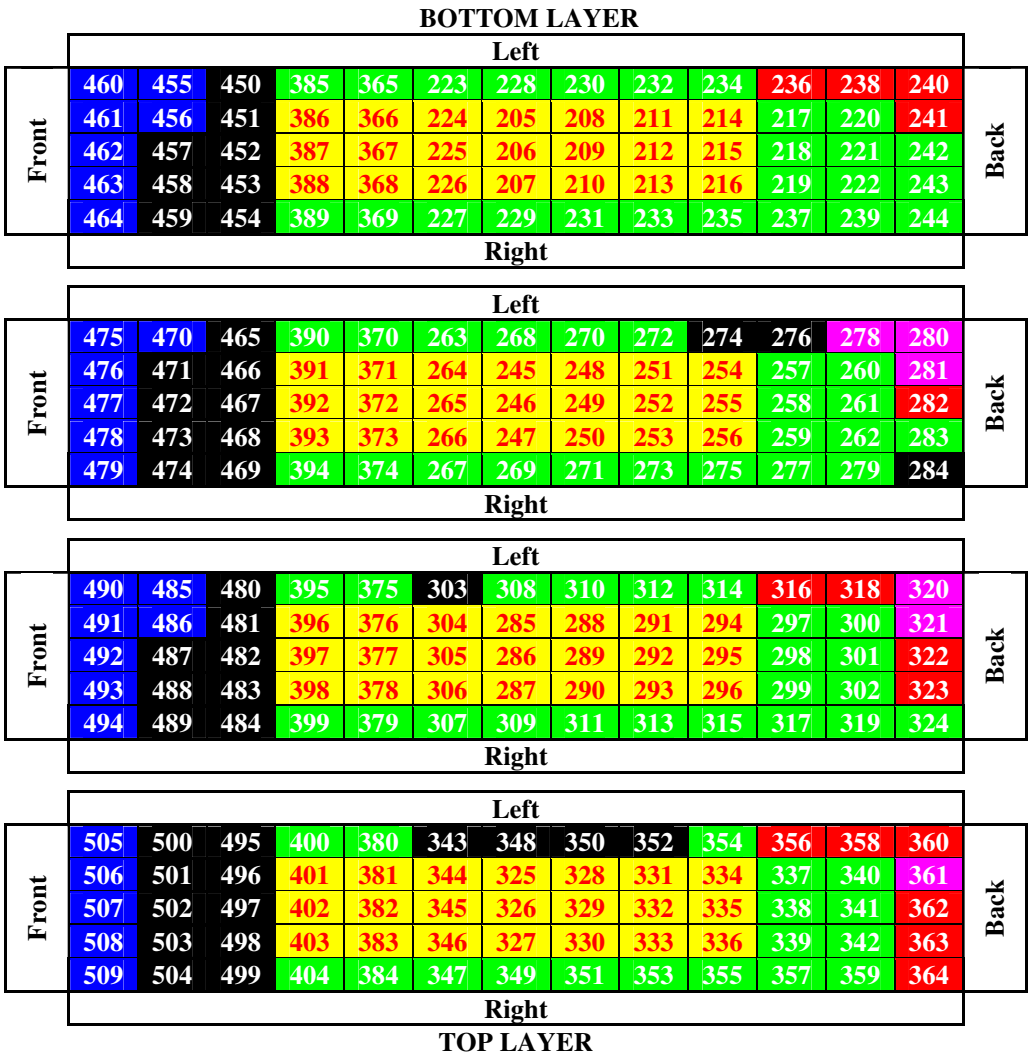


**Fig. 9**: Diagram of progressive slices through the tumor and surrounding cells. Numbers indicate voxel universes for tallying deposited dose. Color scheme: blue (outside universe), black (eye ball); green (eye – aqueous humor); red (fat); pink (optic nerve); yellow (tumor). Each section corresponds to a layer in the z - direction

**Table 1**: Tumor classification for uveal melanoma (Cirrone et al. 2004)

| Lesion Size | Lesion Type or Stage | % Patients Examined |
|---|---|---|
| Diameter < 10 mm and/or thickness ≤ (3 mm) | Small lesions (S) or $T_1$ (TNM) | 2 Patients (4%) |
| Diameter 10-15 mm and/or thickness 4-5 mm | Medium-size lesions (M) or $T_2$ | 17 Patients (36%) |
| Diameter 16 -20 mm and/or thickness 6-10 mm | Large lesions (L) or $T_3$ | 28 Patients (60%) |

Modifications to the lens of the eye were performed as well. In the original voxel phantom, the lens was defined as a series of voxels making up a single universe. This is a valid method for determining effects of radiation dose to the whole lens. However, knowing the dose profile through in the lens of the eye would be an invaluable tool in determining the severity to which the lens was irradiated; if a miscalculation occurs and the patient stares directly into the treatment beam. Therefore, each voxel within the lens was defined as a single independent universe; thus allowing the dose profile to be generated and the maximum and minimum doses in the lens to be calculated. Cross sections of the lens of the eye indicating voxel numbers are shown in Fig. 10.

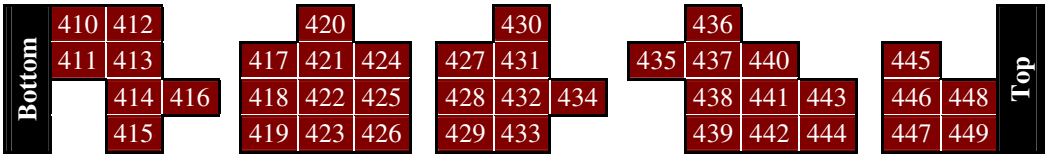


**Fig. 10**: Cross sections of the lens indicating 2.2 x 2.2 x 1.4 mm voxel universe numbers. Each section corresponds to a layer (z-axis) of the lens

As with most proton-therapy treatments a range modifier was needed to adjust the maximum range of the protons. Therefore, one final modification to the phantom was performed. The outside universe surrounding the phantom was converted from air to water thus simulating a water range modifier between the proton source and the eye allowing for maximum dose deposition within the tumor volume.

*Coupling the Beam and the Phantom*

Three situations for proton radiotherapy were modeled and simulated: one ideal and two worst case scenarios. During all simulations the location of the tumor and the orientation of the eye were static; however, the orientation of the beam was varied. During the ideal case, the eye was oriented with the lens of the eye looking up and way from the proton beam to minimize the dose deposited to vital optical tissues while maximizing dose deposition within the tumor volume as shown in Fig. 11.

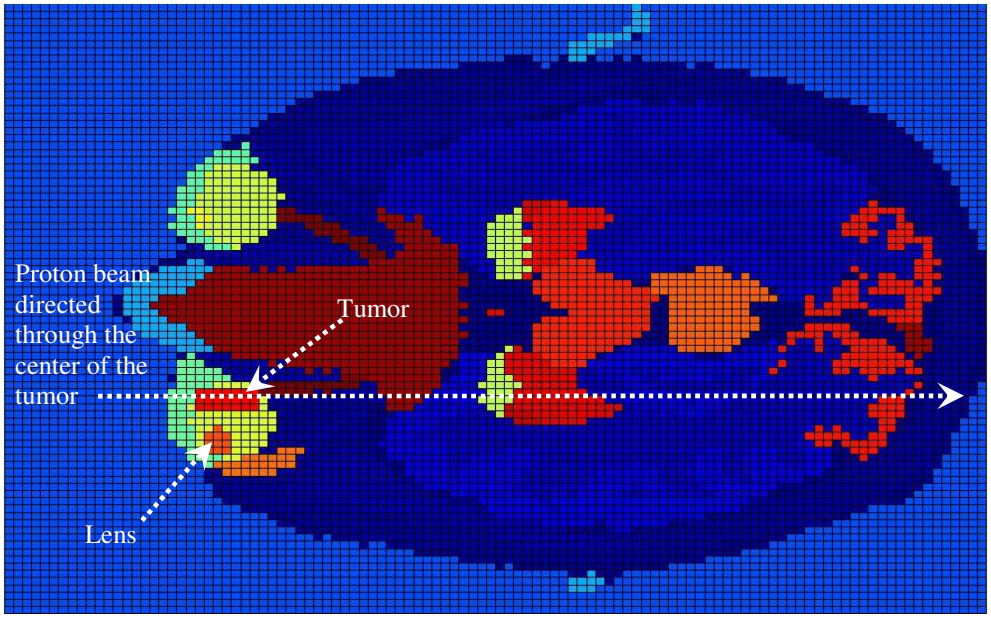


**Fig. 11**: Cross section of the modified Zubal head phantom for the ideal scenario

During the first worst case scenario the lens remained in the same position; however, the proton beam was aimed directly into it. This geometry allowed for the dose deposited in vital regions of the eye to be determined as shown in Fig. 12. This scenario could be a result of a miscalculation with the result being direct radiation of the lens.

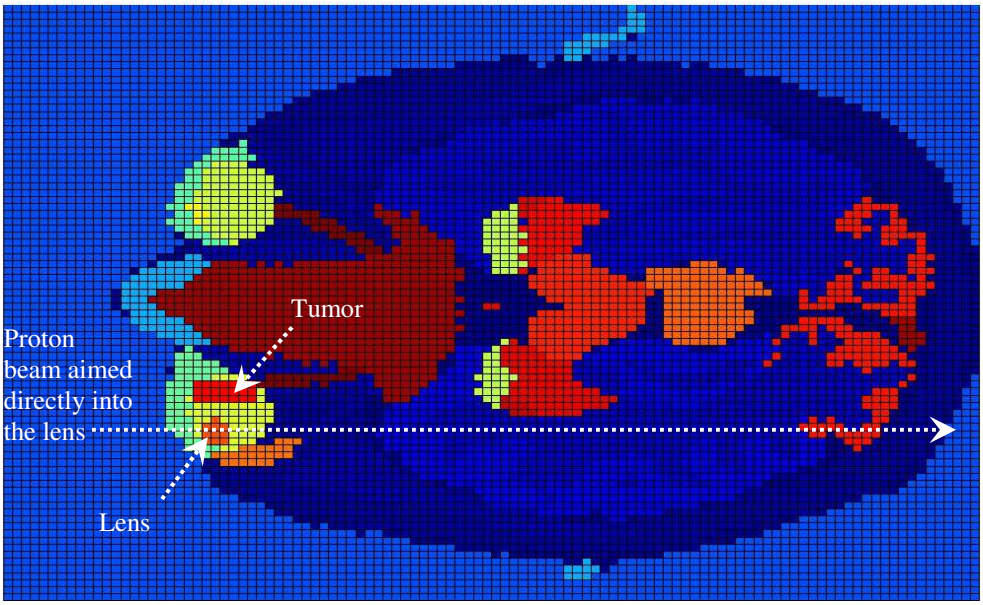


**Fig. 12**: Cross section of the modified Zubal head phantom worst case #1

During the second worst case scenario, the lens of the eye was again oriented looking up and way from the ideal beam trajectory; however, the beam was aimed directly into the bone of the ocular socket as Fig. 13 illustrates. This simulation was performed to determine the deposited dose within the vital tissues of the eye due to scattering.

In all cases the dose deposited due to protons and secondary interactions, multiple coulombic energy scattering, elastic and inelastic scattering, and non-elastic nuclear reactions (i.e., the production of secondary electrons) was calculated. This was

accomplished by tallying energy deposition in units of MeV/g/proton history. A typical proton-therapy treatment for uveal melanoma consists of four treatment sessions delivering a total dose of approximately 50 Gy within the tumor volume. This translates to approximately 12.5 Gy delivered to the tumor volume per treatment (Metz 2006). Therefore, once energy deposition within the tumor was calculated, it was converted to units of Gy/history and multiplied by the appropriate proton fluence required to deposit 12.5 Gy to the tumor volume per fraction. Doses to all tissues for all cases within the modified Zubal phantom were then calculated.

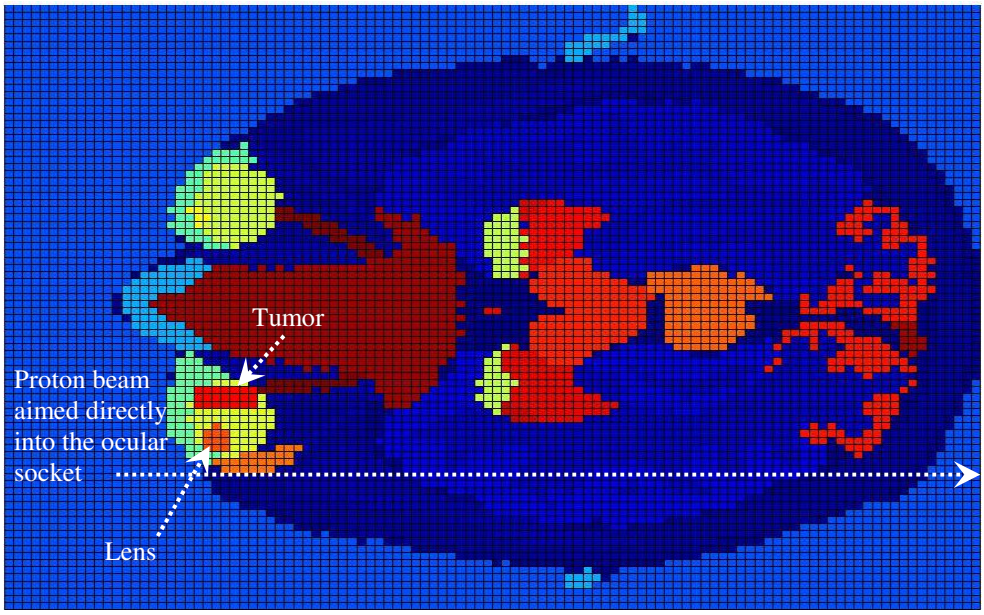


**Fig. 13**: Cross section of the modified Zubal head phantom worst case #2

At high proton energies, interactions of all types are possible. One such interaction is the production of neutrons due to proton interaction with carbon and nitrogen. Therefore, neutron absorbed-dose distributions from the production of neutrons during treatment were calculated for all scenarios.

# CHAPTER III

# RESULTS AND DISCUSSION

*Ideal Case*

Three scenarios were simulated for proton radiotherapy, as previously stated. For all cases the proton SOBP simulated during the benchmark was used and the results compared to those obtained by Oertli (2006). Fig. 14 illustrates the simplified geometry of the human eye developed by Oertli (2006).

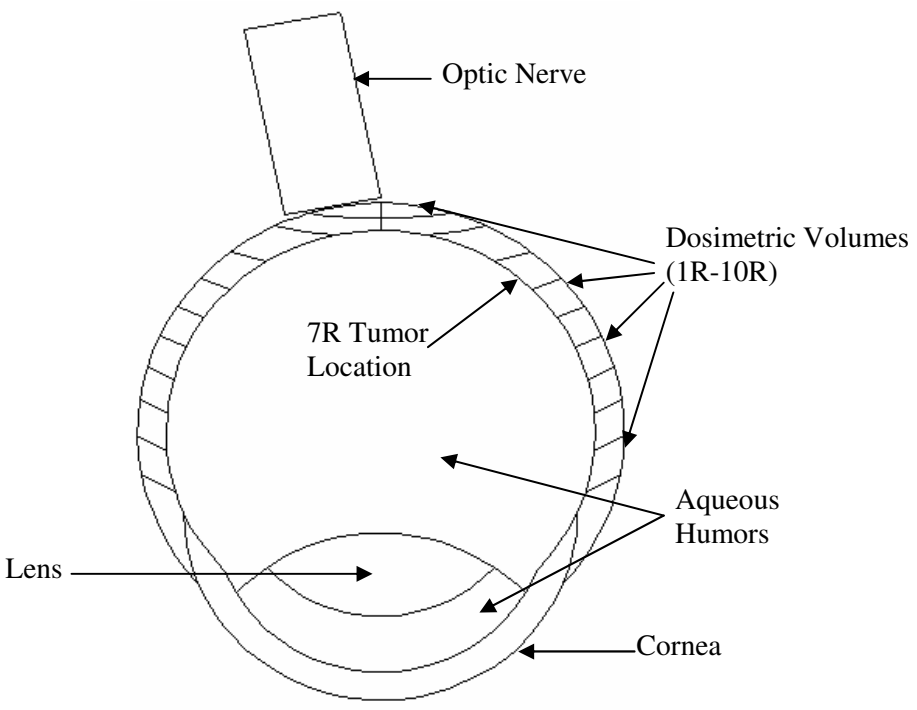


**Fig. 14**: Simplified eye geometry of the human developed by Oertli (Oertli 2006)

Obtaining the dose delivered to various parts of Oertli's (2006) eye was accomplished by subdividing the eye into dosimetric volumes, which include the lens,

cornea, anterior and vitreous humors, and a series of volumes in the eye wall (Oertli 2006). Due to the size of the voxels the anterior and vitreous humors over lap in the voxel map; therefore, the terms will be used interchangeably from this point forward. These volumes are illustrated in Fig. 14 (above).

Typical case simulations were performed using the simplified eye model and the complex Zubal phantom and comparisons made. During the typical scenario the proton beam was directed into the tumor volume; thus maximizing dose within the lesion and minimizing dose to vital tissues as illustrated in Fig 15.

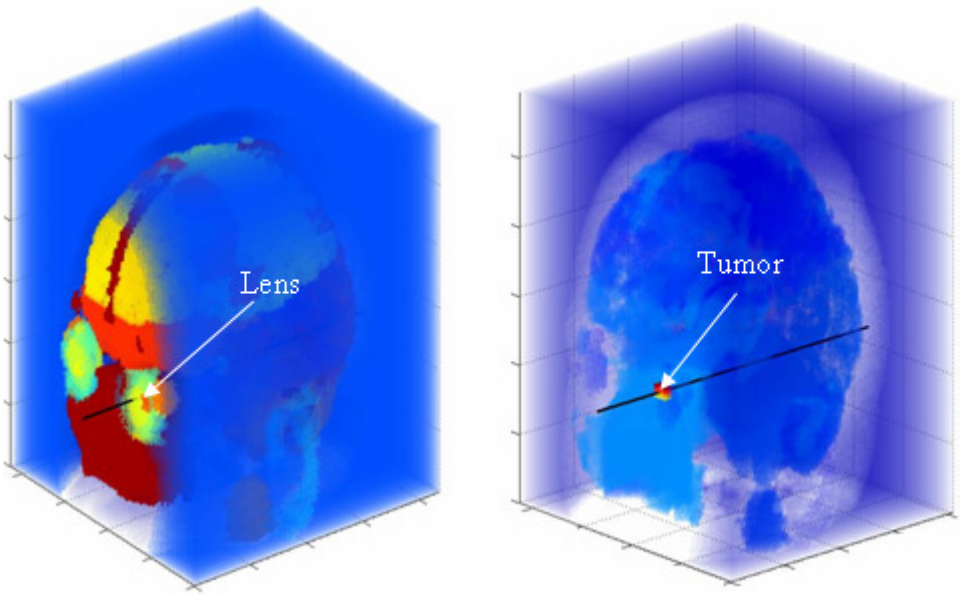


**Fig. 15**: Ideal case: proton beam missing the lens (left) and directed into the center of the tumor (right)

As previously stated, a typical proton therapeutic dose for uveal melanoma is about 50 Gy delivered over four fractions (12.5 Gy per fraction) (Metz 2006). Therefore, all simulations were optimized to deliver a dose of 12.5 Gy per fraction to the tumor

volume while minimizing dose elsewhere. The results for the typical treatment scenario obtained using the simplified and complex geometries are shown in Table 2.

**Table 2:** Dose deposition comparison for a typical treatment scenario

| **Oertli's Phantom (2006)** | | | **Modified Zubal phantom** | | |
|---|---|---|---|---|---|
| **Dose Volume** | **Dose per Fraction (Gy)** | **Total Dose (Gy)** | **Dose Volume** | **Dose per Fraction (Gy)** | **Total Dose (Gy)** |
| Cornea | 0.60 | 2.41 | Cornea | 0.42 | 1.68 |
| Anterior/Vitreous humor | 5.02 | 20.1 | Anterior/Vitreous humor | 4.09 | 16.36 |
| Lens | 0.09 | 0.36 | Lens | 0.0021 | 0.0082 |
| Optic Nerve | 1.06 | 4.26 | Optic Nerve | 0.0686 | 0.2742 |
| Eye Wall | 73.85 | 295.38 | Eye Wall | 3.52 | 14.06 |
| Tumor | 12.50 | 50.00 | Tumor | 12.50 | 50.00 |

Results indicate that doses to all vital tissues for both models were within acceptable limits. Doses to the lens were 0.09 and 0.0021 Gy/fraction for the simplified and complex geometries, respectively. These doses are well below the acceptable limit of less than 8 Gy – 10 Gy to the lens (Jones and Errington 2000). Similarly, doses to the optic nerve were 1.06 and 0.0082 Gy per fraction, respectively, which is below the acceptable the limit of 10 Gy to the optic nerve (Jones and Errington 2000). For each treatment, the cornea received 0.6 and 0.42 Gy per fraction, respectively, which is well within the acceptable limit of 15 Gy (Simonva 2002). For the ideal case, the cumulative dose to the lens was 0.36 and 0.0082 Gy, while the dose within the tumor was the prescribed 50 Gy per four fractions.

Although both simulations produced acceptable results, differences between the two models were evident. First, for the complex geometry, the lens of the eye was divided into individual 2.2 x 2.2 x 1.4 mm voxel universes to illustrate the maximum and

minimum dose deposition within the lens. Fig. 16 shows the dose distribution within the lens of the eye for all layers.

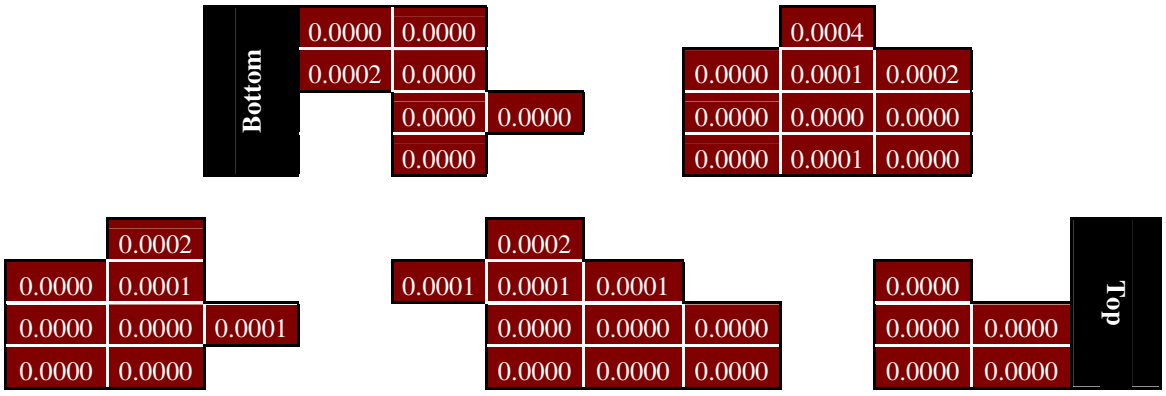


**Fig. 16**: Dose (Gy) distribution for the typical case scenario through the lens of the modified Zubal phantom (read left to right). Each section corresponds to a layer (z-axis) of the lens

As demonstrated above, the maximum and minimum doses were 0.0004 and 0.0000 Gy, respectively, which is well below the acceptable limit.

Secondly, the tumor in the complex geometry was separated into individual voxel universes producing a dose distribution across the tumor volume, as illustrated by Fig. 17. Here, the white on blue color scheme indicates the tumor volume while the red on black illustrates the surrounding tissues. The cross-sections of the tumor clearly illustrate the Bragg peak occurring within the tumor volume, which is an invaluable tool when designing proton therapy treatments. Using the simplified model, one is unable to obtain a dose distribution throughout the tumor volume, thus illustrating the superiority of the complex model.


**Fig. 17**: Cross section representation (bottom to top) illustrating the dose distribution (Gy/fraction) across the tumor volume. Each section corresponds to a layer (z-axis) of the tumor

The location and size of the tumor also differs between the two models. In the simplified model the tumor was located in the wall (choroid or sclera) of the eye with a volume of 0.822 $cm^3$ while in the complex geometry the tumor was located in the vitreous humor with a volume of 8.12 $cm^3$. The location of the tumor had little effect on

the dose distribution throughout the eye and the tumor; however, the volume can greatly affect energy deposition curves within the tumor volume.

The tumor size used in Oertli's (2006) simplified model was small compared to the SOBP created by the energy distribution used. The energy distribution used generated a SOBP that occurred over a range of 15 mm as illustrated in Fig 18.

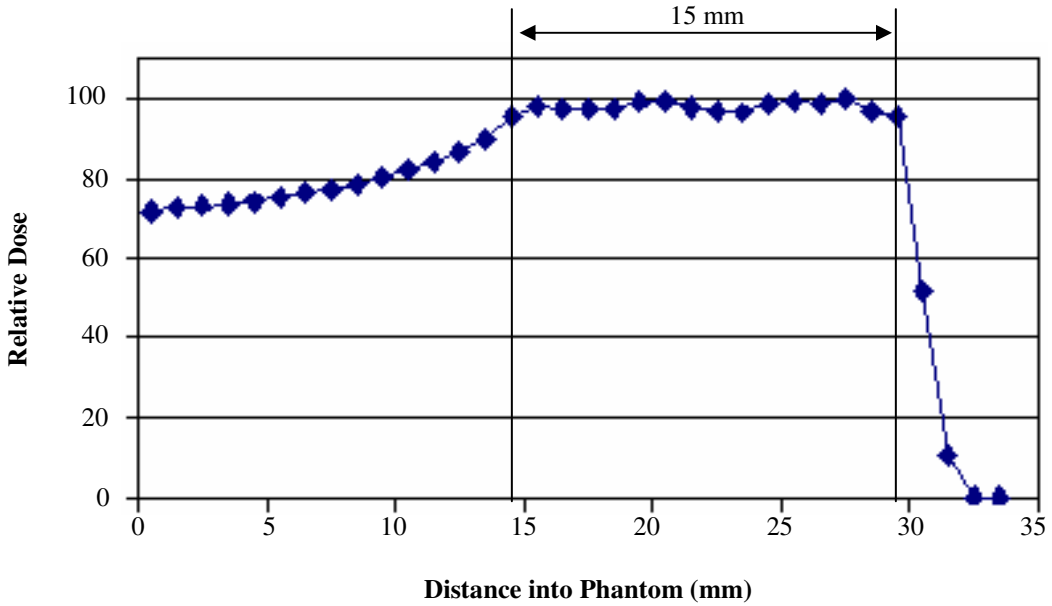


**Fig. 18**: SOBP obtained using the energy distribution from Oertli (2006)

Although a range modifier was used in Oertli's (2006) model, it did not affect the size of the SOBP. It merely shifted it to a shallower depth into the phantom. The dose deposition from the front and rear walls of the simplified geometry indicated that the SOBP occurred over the entire eye and was not confined to the tumor volume. Table 3 shows the dose distribution throughout the dosimetric volumes of the eye wall defined by Oertli (2006). The dose ranges from a 43.45 Gy maximum in the front of the eye wall to a 40.89 Gy maximum at the back of the eye wall with 50.01 Gy to the tumor (7R –

middle of the eye wall). This dose distribution clearly indicates that the SOBP occurred over the entire right eye wall.

**Table 3**: Dose distribution in the right eye wall as defined by Oertli (2006)

| Dose Volume | Dose per Fraction (Gy) | Total Dose (Gy) |
|---|---|---|
| 2R | 10.86 | 43.45 |
| 3R | 10.25 | 40.99 |
| 4R | 9.71 | 38.85 |
| 5R | 9.67 | 38.7 |
| 6R | 10.51 | 42.02 |
| 7R | 12.5 | 50.01 |
| 8R | 10.22 | 40.89 |
| 9R | 1.56 | 6.23 |
| 10R | 0.02 | 0.09 |

Because the SOBP occurred over a large volume and was not confined within the tumor, a high proton fluence was necessary to deposit the prescribed 12.5 Gy within the tumor volume for Oertli's (2006) model. The high fluence used resulted in unusually high doses to areas surrounding the tumor volume as shown in Table 3 (above). The effects of the large fluence are more evident during worst case simulations.

Fig. 19 and Fig. 20 are graphical representations of the Bragg peak occurring within the tumor volume for the complex model.

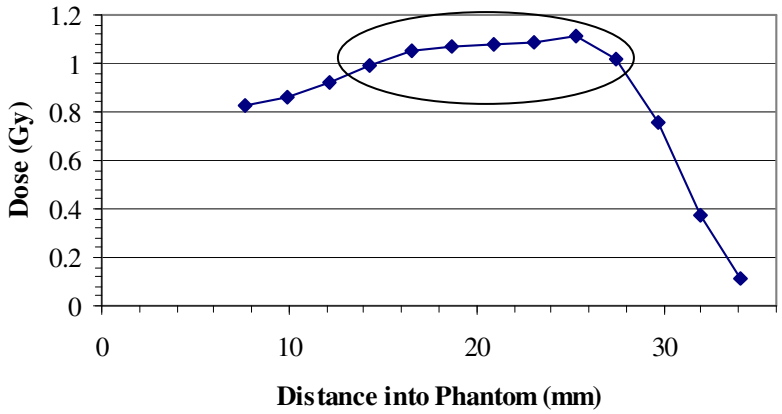


**Fig. 19**: Ideal case SOBP through the center of the tumor. Circled data points are within the tumor volume

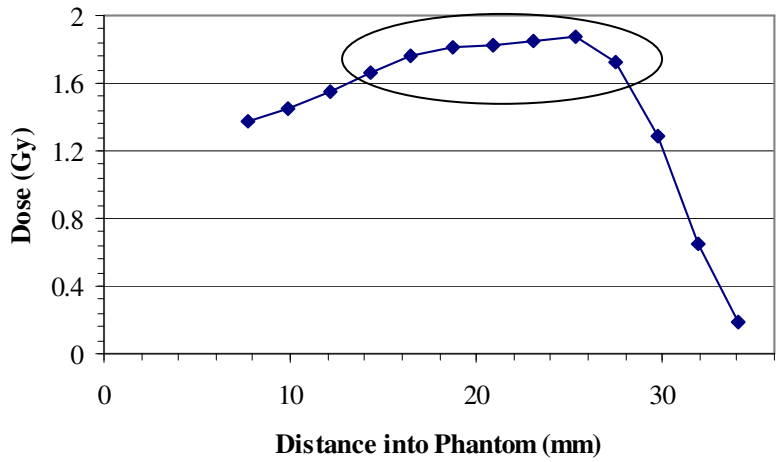


**Fig. 20:** Ideal case total dose deposition SOBP. Circled data points are within the tumor volume

Although the Bragg peak occurs within the tumor volume for the complex model, there are discrepancies between the data obtained and the expected values as illustrated in Fig. 21.

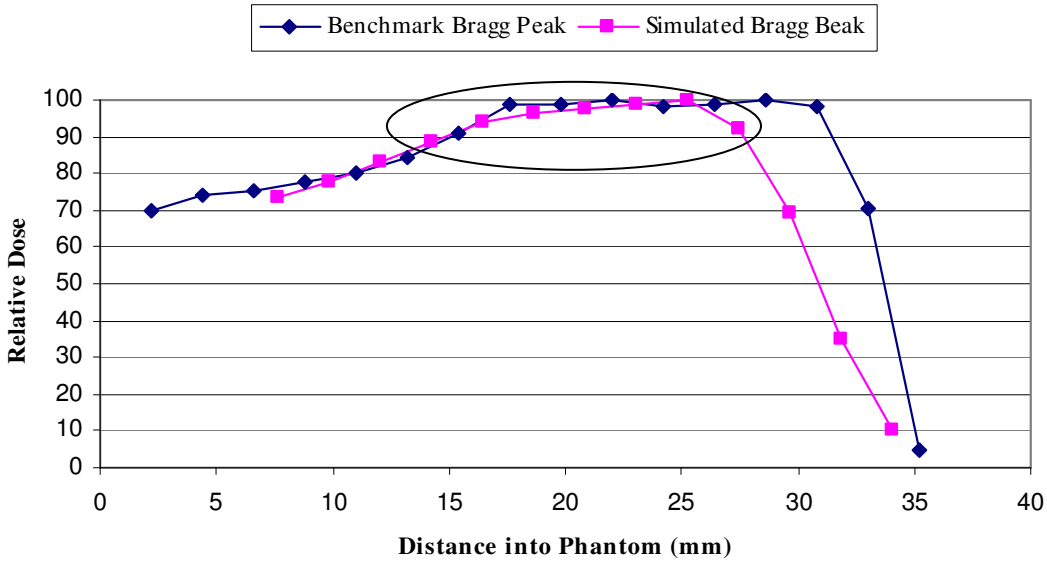


**Fig. 21**: Benchmark Bragg peak vs. simulated Bragg peak (ideal case). Circled data points (pink) are within the tumor

As illustrated, data points at the beginning of the Bragg peak are lower than expected values and the entire plot is shifted to the left (i.e., dose deposition occurs at a greater rate than the benchmark suggests). These discrepancies are explained by three phenomena:

- Resolution of the dose distribution
- Scattering effects
- Varying densities of the tissues within the eye

The relatively large size of the voxels (2.2 x 2.2 x 1.4 mm) limits the resolution of the deposited dose within each voxel because the dose is averaged over the entire voxel volume; therefore, obtaining data points at smaller intervals is impossible. Additionally, scattering occurs within and outside of each voxel. If an interaction occurs on or near a voxel border, the scattered particles are likely to be scattered outside of the sensitive volume resulting in lower than expected dose deposition. Furthermore, the densities of the tissues within the eye are not constant. Most tissues within the eye have a density

greater than that of water (the material used for benchmarking); therefore, the protons undergo more interactions and lose energy faster than the benchmark scenario suggests. Greater energy deposition per unit path length traveled by the proton would cause the proton to lose all of its energy at a faster rate and explain why the SOBP shifts to the left.

Another major difference between the two models is the complexity of the modified Zubal phantom. The simple phantom contains six structures of the human eye whereas the modified Zubal phantom models 29 critical structures of the human head. Table 4 shows the dose deposited within these 29 voxel universes. As demonstrated, there is little or no residual dose to tissues behind or near the affected eye. The dose profile of protons allows for maximum dose deposition within the tumor volume while sparing healthy tissues around the lesion. However, at high proton energies interactions of all types are possible. The doses that were recorded in tissues behind the eye are a result of one such interaction; (p,n) interactions with carbon, oxygen and nitrogen atoms within the tissues of the eye produce secondary neutrons which deposit dose along their path. Due to their neutral charge, secondary neutrons have a long range and fewer interactions with nearby atoms. Therefore, the neutron dose can be deposited relatively far from the initial interaction that produced the neutron. For this reason, neutron absorbed-dose values to all tissues for all cases were calculated. Fig. 22 and Fig. 23 show the neutron absorbed-dose values obtained for the ideal case in the lens of the eye and the tumor, respectively.

**Table 4**: Neutron dose deposition within tissues of the modified Zubal phantom (ideal case)

| Cell # | Tissue | Dose (Gy) |
|---|---|---|
| 1 | Skin | $8.63 \times 10^{-6}$ |
| 2 | cerebral fluid | $6.11 \times 10^{-9}$ |
| 3 | Fat | $7.33 \times 10^{-6}$ |
| 4 | skeletal bone | $1.65 \times 10^{-8}$ |
| 5 | skeletal muscle | $6.59 \times 10^{-6}$ |
| 6 | white matter (left) | 0.00 |
| 8 | temporal lobe (left) | 0.00 |
| 9 | temporal lobe (right) | 0.00 |
| 10 | spinal cord | 0.00 |
| 26 | bone marrow | 0.00 |
| 30 | Cartilage | $2.77 \times 10^{-7}$ |
| 40 | internal capsule (left) | 0.00 |
| 41 | internal capsule (right) | 0.00 |
| 42 | Septum pellucidium | 0.00 |
| 43 | Thalamus (left) | 0.00 |
| 44 | Thalamus (right) | 0.00 |
| 48 | motor cortex (left) | 0.00 |
| 49 | motor cortex (right) | 0.00 |
| 50 | falx cerebri | 0.00 |
| 51 | parietal lobe (left) | 0.00 |
| 52 | parietal lobe (right) | 0.00 |
| 55 | amygdala (left) | 0.00 |
| 56 | amygdala (right) | 0.00 |
| 59 | Globus pallidus (left) | 0.00 |
| 60 | Globus pallidus (right) | 0.00 |
| 63 | prefrontal lobe (left) | 0.00 |
| 64 | prefrontal lobe (right) | 0.00 |
| 72 | Parotid gland (left) | 0.00 |
| 73 | Parotid gland (right) | 0.00 |
| 74 | Lacrimal gland (left) | 0.00 |
| 75 | Lacrimal gland (right) | 0.00 |
| 76 | cerebellum (white matter) | 0.00 |
| 77 | cerebellum (cortex) | 0.00 |
| 80 | medulla oblongata | 0.00 |
| 81 | Frontal lobe (left) | 0.00 |
| 82 | Frontal lobe (right) | $4.49 \times 10^{-8}$ |
| 83 | Pons | 0.00 |
| 84 | Occipital lobe (left) | 0.00 |
| 85 | Occipital lobe (right) | 0.00 |
| 86 | hippocampus (left) | 0.00 |
| 87 | hippocampus (right) | 0.00 |
| 88 | Pituitary gland | 0.00 |
| 89 | uncus (left) | 0.00 |
| 90 | uncus (right) | 0.00 |
| 91 | caudate nucleus (left) | 0.00 |
| 92 | caudate nucleus (right) | 0.00 |
| 93 | insula cortex (left) | 0.00 |
| 94 | insula cortex (right) | 0.00 |
| 95 | Sinuses | $3.8 \times 10^{-7}$ |
| 96 | Putamen (left) | 0.00 |
| 97 | Putamen (right) | 0.00 |

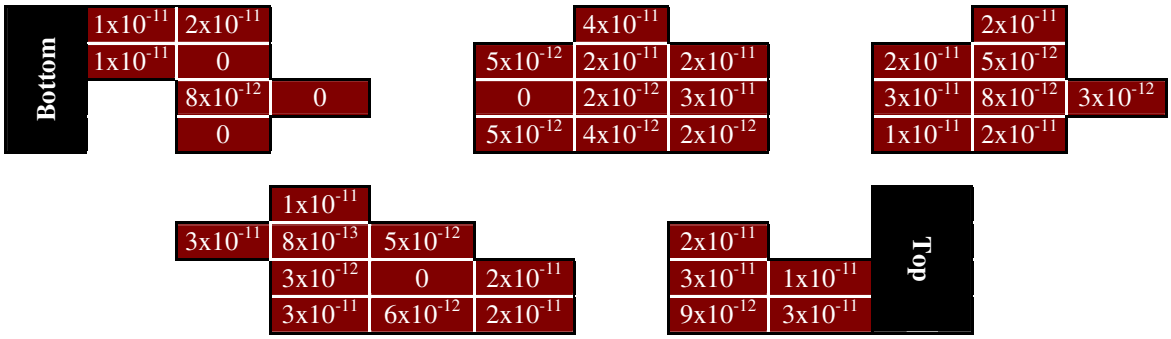


**Fig. 22**: Neutron absorbed-dose (Gy) distribution through the lens of the eye read from left to right (ideal case). Each section corresponds to a layer (z-axis) of the lens

As expected, neutron absorbed-dose values were very low. For the ideal case scenario only 758 neutrons were produced during the simulation. Throughout the phantom neutron absorbed-dose values for all tissues were as expected. Once again the complex modified Zubal phantom produced a dose distribution through the tumor that could not be produced with a simple geometry phantom.

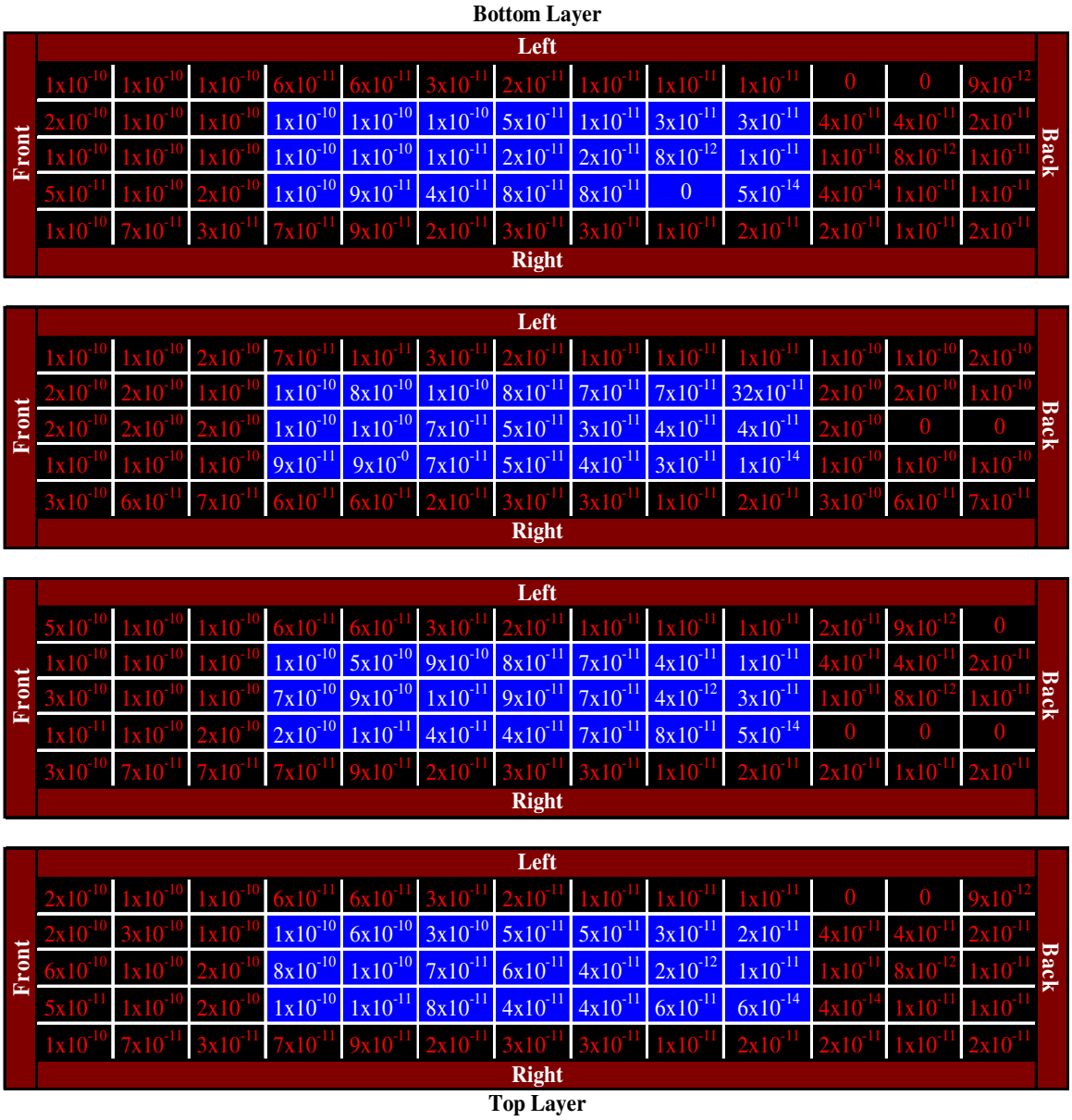


**Fig. 23**: Neutron absorbed-dose (Gy) distribution through the tumor (ideal case). Each section corresponds to a layer (z-axis) of the tumor

*Worst Case Scenario – Lens*

Two worst case simulations were performed using the complex Zubal phantom. However, due to the limited capabilities of the simplified eye model, comparisons were made for only one scenario.

The lens of the eye is a highly radiosensitive organ that is surrounded by cuboid cells which are also very radiosensitive. Coagulation of proteins within the lens occurs at doses greater than 2 Gy resulting in visual impairments such as cataract (IAEA 2007). Due to the radiosensitive characteristics of the lens, a worst case simulation mimicking a patient starring directly into the treatment beam during therapy was performed. Fig. 24 illustrates the orientation of the lens of the eye with respect to the proton beam for the lens worst case scenario.

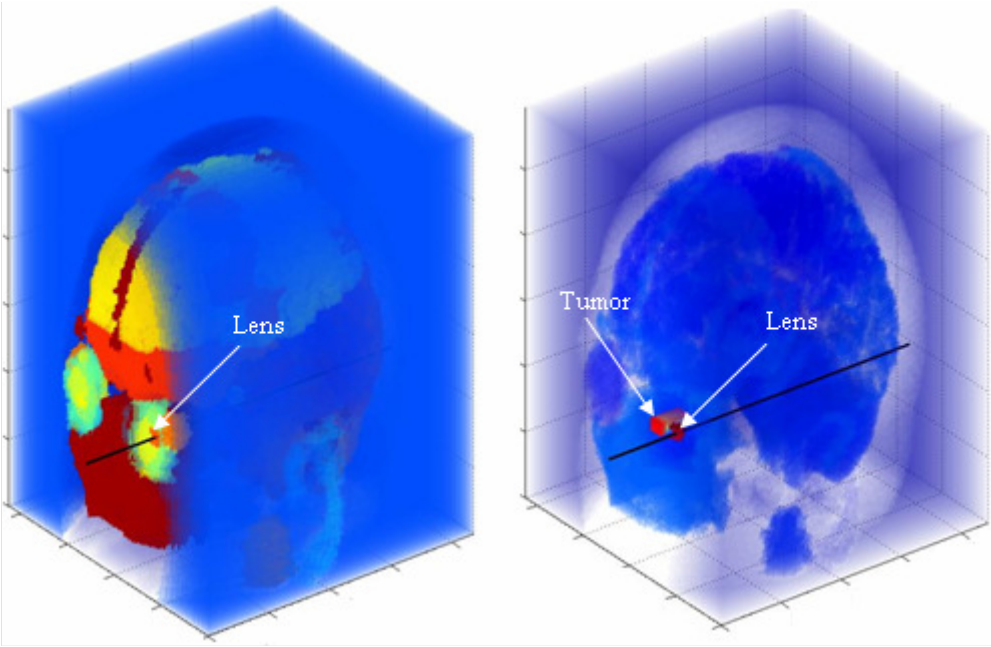


**Fig. 24**: Lens worst case: proton beam directly into the lens (left) and missing the tumor (right)

The results for the direct irradiation of the lens obtained using the simplified and complex geometries are shown in Table 5. Because this simulation mimicked a patient gazing into the beam during treatment, the same dose profile, number of proton histories (300,000) and proton fluence from the typical treatment scenario was used.

**Table 5:** Dose deposition comparison for a worst case (lens) treatment scenario

| Oertli's Phantom (2006) | | | Modified Zubal phantom | | |
|---|---|---|---|---|---|
| **Dose Volume** | **Dose per Fraction (Gy)** | **Total Dose (Gy)** | **Dose Volume** | **Dose per Fraction (Gy)** | **Total Dose (Gy)** |
| Cornea | 9.02 | 36.08 | Cornea | 4.26 | 17.04 |
| Anterior/Vitreous humor | 31.34 | 125.36 | Anterior/Vitreous humor | 4.87 | 19.48 |
| Lens | 38.72 | 154.88 | Lens | 5.99 | 20.77 |
| Optic Nerve | 0.00 | 0.00 | Optic Nerve | 0.00 | 0.00 |
| Eye Wall | 0.81 | 3.24 | Eye Wall | 0.60 | 2.40 |
| Tumor | 0.00 | 0.00 | Tumor | 0.01 | 0.02 |

As discussed earlier, a high proton fluence was used to deposit the prescribed 12.5 Gy within the tumor volume for Oertli's (2006) ideal case. As shown in Table 5 (above), the effects of the large fluence resulted in unnecessarily large doses to vital tissues of the eye during the worst case simulation. Although doses above the threshold values were observed for both phantoms, Oertli's (2006) simulation resulted in extremely high doses, which would result in sure vision loss.

Results indicate that doses to vital tissues were above acceptable limits. Total doses to the lens were 154.88 and 20.77 Gy for the simplified and complex geometry, respectively. These doses are well above the acceptable limit of 8 – 10 Gy to the lens (Jones and Errington 2000). Fig. 25 illustrates the dose distribution through the lens of the eye for the modified Zubal simulation.

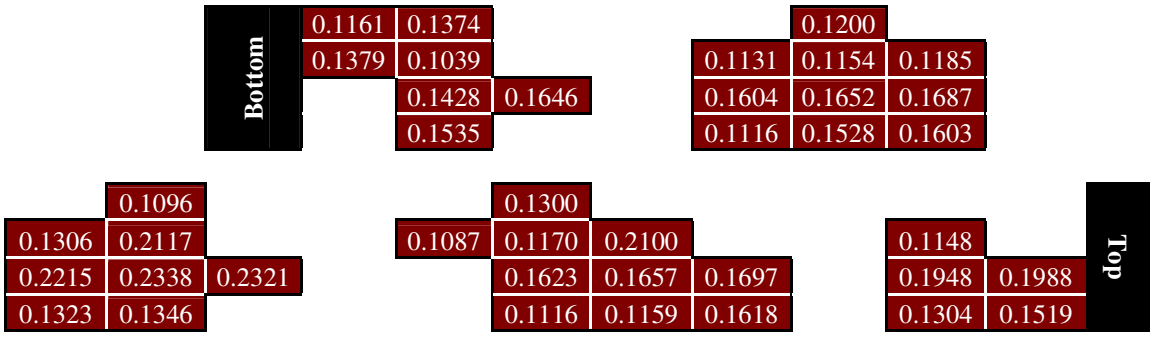


**Fig. 25**: Dose distribution (Gy/fraction) through the lens for the worst case scenario (lens) and is read left to right. Each section corresponds to a layer (z-axis) of the lens

The cross-sections depicted above illustrate the severity of the dose deposition within the lens of the eye. The maximum and minimum doses to the lens of the eye were 0.2338 and 0.1039 Gy, respectively. On average, 0.1498 Gy was deposited per voxel (6.776 $mm^3$) of the lens. Therefore, because the lens is very radiosensitive and detrimental effects occur at recorded doses (greater than 2Gy), visual impairments such as cataract are imminent. The cross-section of the lens of the eye also allows for a dose reconstruction to be performed in the event of direct irradiation of the lens. A dose reconstruction cannot be performed with the simplified model discussed herein; thus illustrating the superiority of the complex geometry.

The optic nerve received 0.00 Gy for both simulations which is below the acceptable the limit of 10 Gy (Jones and Errington 2000). This result is not surprising. Although the optic nerve was directly in the path of the proton beam for each simulation, the proton energy was not great enough for the protons to reach the optic nerve before depositing all of their energy. For each treatment, the cornea received 36.08 and 17.04 Gy, respectively, which is well above the acceptable limit of 15 Gy (Simonova 2002). One would expect severe visual impairments at doses recorded for this worst case

scenario. Coagulation of proteins within the lens would likely occur resulting in visual impairments such as cataracts. Doses to the tumor volume were 0.00 and 0.02 Gy for the simplified and complex geometries, respectively.

As previously stated, (p,n) interactions with carbon, oxygen and nitrogen atoms within the tissues of the eye are likely at high proton energies. As a result secondary neutrons can deposit dose within tissues outside the region of interest. For this reason, neutron absorbed-dose values to all tissues are presented here. Fig. 26 and Fig. 27 show the neutron absorbed-dose distribution obtained for this worst case in the lens of the eye and the tumor, respectively. As expected, neutron absorbed-dose values for direct irradiation of the lens were very low. For this scenario, only 752 neutrons were produced during the simulation. Throughout the phantom, neutron absorbed-dose values for all tissues were as expected. Again the complex modified Zubal phantom demonstrated its superiority by producing a dose distribution through the lens and tumor that could not be produced with a simple geometry phantom.

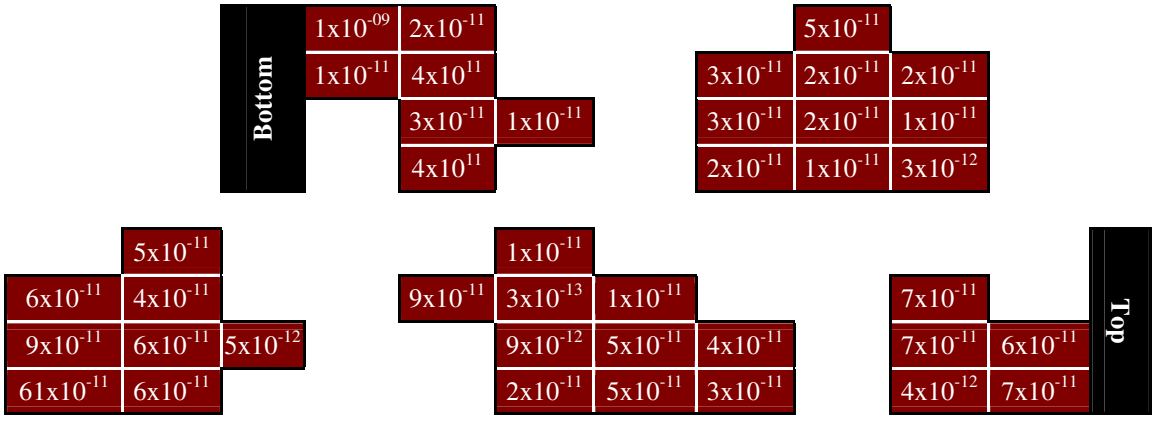


**Fig. 26**: Neutron absorbed-dose (Gy) distribution through the lens of the eye (worst case). Each section corresponds to a layer (z-axis) of the lens

**Bottom Layer**

| Front | Left | | | | | | | | | | | | Back |
|---|---|---|---|---|---|---|---|---|---|---|---|---|---|
| | $3x10^{-11}$ | $1x10^{-11}$ | $1x10^{-13}$ | $4x10^{-12}$ | $8x10^{-15}$ | $3x10^{-16}$ | $1x10^{-16}$ | 0 | 0 | $1x10^{-11}$ | 0 | 0 | 0 |
| | $2x10^{-11}$ | $2x10^{-11}$ | $1x10^{-11}$ | $2x10^{-12}$ | $1x10^{-11}$ | 0 | 0 | 0 | $5x10^{-12}$ | $2x10^{-11}$ | $4x10^{-11}$ | 0 | 0 |
| | $2x10^{-11}$ | $1x10^{-11}$ | $1x10^{-14}$ | $2x10^{-11}$ | $1x10^{-11}$ | $3x10^{-12}$ | 0 | 0 | $2x10^{-11}$ | $1x10^{-11}$ | $1x10^{-11}$ | $8x10^{-12}$ | 0 |
| | $1x10^{-11}$ | $4x10^{-12}$ | $2x10^{-11}$ | $3x10^{-11}$ | $4x10^{-11}$ | $2x10^{-12}$ | $2x10^{-12}$ | $6x10^{-11}$ | 0 | 0 | $4x10^{-14}$ | 0 | 0 |
| | $3x10^{-11}$ | $6x10^{-11}$ | $3x10^{-11}$ | $3x10^{-11}$ | $5x10^{-11}$ | $3x10^{-11}$ | $7x10^{-11}$ | $2x10^{-11}$ | $1x10^{-11}$ | $6x10^{-11}$ | $2x10^{-11}$ | $1x10^{-11}$ | 0 |
| | Right | | | | | | | | | | | | |

| Front | Left | | | | | | | | | | | | Back |
|---|---|---|---|---|---|---|---|---|---|---|---|---|---|
| | $1x10^{-11}$ | $4x10^{-12}$ | $8x10^{-15}$ | 0 | 0 | $6x10^{-15}$ | $3x10^{-11}$ | $1x10^{-11}$ | $1x10^{-11}$ | $6x10^{-15}$ | $1x10^{-10}$ | $1x10^{-10}$ | 0 |
| | $1x10^{-11}$ | $2x10^{-12}$ | $1x10^{-11}$ | 0 | 0 | 0 | $2x10^{-11}$ | 0 | 0 | $5x10^{-12}$ | $2x10^{-10}$ | 0 | 0 |
| | $4x10^{-11}$ | $2x10^{-11}$ | $1x10^{-11}$ | $3x10^{-12}$ | $3x10^{-12}$ | $2x10^{-11}$ | $2x10^{-11}$ | 0 | $4x10^{-11}$ | $2x10^{-11}$ | $2x10^{-10}$ | 0 | 0 |
| | $6x10^{-11}$ | $3x10^{-11}$ | $4x10^{-11}$ | $2x10^{-12}$ | $2x10^{-12}$ | 0 | $1x10^{-11}$ | $4x10^{-12}$ | $6x10^{-11}$ | 0 | $1x10^{-10}$ | $1x10^{-10}$ | 0 |
| | $2x10^{-11}$ | $3x10^{-11}$ | $5x10^{-11}$ | $3x10^{-11}$ | $7x10^{-11}$ | $1x10^{-11}$ | $3x10^{-11}$ | $6x10^{-11}$ | $2x10^{-11}$ | $1x10^{-11}$ | $3x10^{-10}$ | $6x10^{-11}$ | $7x10^{-11}$ |
| | Right | | | | | | | | | | | | |

| Front | Left | | | | | | | | | | | | Back |
|---|---|---|---|---|---|---|---|---|---|---|---|---|---|
| | $5x10^{-12}$ | $3x10^{-16}$ | $1x10^{-16}$ | $7x10^{-12}$ | 0 | $1x10^{-11}$ | $4x10^{-12}$ | $8x10^{-15}$ | $1x10^{-11}$ | $1x10^{-11}$ | $2x10^{-11}$ | $9x10^{-12}$ | 0 |
| | $8x10^{-12}$ | 0 | 0 | $4x10^{-13}$ | $1x10^{-11}$ | $2x10^{-11}$ | $2x10^{-12}$ | $1x10^{-11}$ | $2x10^{-11}$ | $1x10^{-11}$ | 0 | 0 | $2x10^{-11}$ |
| | $1x10^{-11}$ | $3x10^{-12}$ | $3x10^{-12}$ | 0 | 0 | $1x10^{-11}$ | $2x10^{-11}$ | $1x10^{-11}$ | 0 | 0 | $1x10^{-11}$ | $8x10^{-12}$ | $1x10^{-11}$ |
| | $3x10^{-11}$ | $2x10^{-12}$ | $2x10^{-12}$ | $3x10^{-12}$ | $7x10^{-12}$ | $4x10^{-12}$ | $3x10^{-11}$ | $4x10^{-11}$ | $4x10^{-12}$ | $6x10^{-11}$ | 0 | 0 | 0 |
| | $7x10^{-11}$ | $3x10^{-11}$ | $7x10^{-11}$ | $7x10^{-12}$ | $1x10^{-11}$ | $6x10^{-11}$ | $3x10^{-11}$ | $5x10^{-11}$ | $6x10^{-11}$ | $2x10^{-11}$ | $2x10^{-11}$ | $1x10^{-11}$ | $2x10^{-11}$ |
| | Right | | | | | | | | | | | | |

| Front | Left | | | | | | | | | | | | Back |
|---|---|---|---|---|---|---|---|---|---|---|---|---|---|
| | $7x10^{-12}$ | $3x10^{-11}$ | $6x10^{-15}$ | $1x10^{-11}$ | $3x10^{-11}$ | $1x10^{-11}$ | $6x10^{-15}$ | 0 | $1x10^{-16}$ | $1x10^{-11}$ | 0 | 0 | 0 |
| | $4x10^{-13}$ | $1x10^{-11}$ | $5x10^{-12}$ | $2x10^{-11}$ | $2x10^{-11}$ | $2x10^{-11}$ | $5x10^{-12}$ | 0 | 0 | $1x10^{-11}$ | 0 | 0 | 0 |
| | 0 | 0 | $2x10^{-11}$ | $1x10^{-11}$ | $2x10^{-11}$ | $1x10^{-11}$ | $2x10^{-11}$ | $3x10^{-12}$ | $3x10^{-12}$ | $4x10^{-11}$ | $1x10^{-11}$ | 0 | $1x10^{-11}$ |
| | $3x10^{-12}$ | $7x10^{-12}$ | $7x10^{-12}$ | $4x10^{-12}$ | $1x10^{-11}$ | $4x10^{-12}$ | $7x10^{-12}$ | $2x10^{-12}$ | 0 | $6x10^{-11}$ | $4x10^{-14}$ | $1x10^{-11}$ | $1x10^{-11}$ |
| | $7x10^{-12}$ | $1x10^{-11}$ | $1x10^{-11}$ | $6x10^{-11}$ | $3x10^{-11}$ | $6x10^{-11}$ | $1x10^{-11}$ | $3x10^{-11}$ | $7x10^{-11}$ | $2x10^{-11}$ | $2x10^{-11}$ | $1x10^{-11}$ | $2x10^{-11}$ |
| | Right | | | | | | | | | | | | |

**Top Layer**

**Fig. 27**: Neutron absorbed-dose (Gy) distribution through the tumor (lens worst case). Each section corresponds to a layer (z-axis) of the tumor

*Worst Case Scenario – Optical Socket*

A second worst case scenario was performed in which the proton beam was directed into the ocular socket of the eye. During this simulation the lens of the eye was oriented looking up and away from the ideal treatment scenario; however, the beam was aimed into the ocular socket nearest to the lens as Fig. 28 illustrates. For this simulation, secondary interactions, multiple coulombic energy scattering, elastic and inelastic scattering, and non-elastic nuclear reactions (i.e., the production of secondary electrons) were included. Comparison between the two geometries was not possible due to the simplicities of Oertli's (2006) model. The purpose of this simulation was to determine the significance of the dose deposition within the vital tissues of the eye due to scattering. Because of its higher density, one would expect more interactions and thus more scattering events within the bone of the ocular socket as opposed to the tissues of the eye. As previously stated; however, MCNPX is unable to track low-energy electrons (<1 keV) and low-energy protons (< 1MeV). Although low doses were expected within the eye, the dose distribution through the eye was lower than expected. This is because scattered electrons and protons less than 1 keV and 1 MeV, respectively, were neglected. It is expected that the majority of the dose deposited during this simulation is due to secondary neutron production during (p,n) reactions as discussed earlier. Table 6 shows the doses to vital tissues of the eye obtained during this simulation.

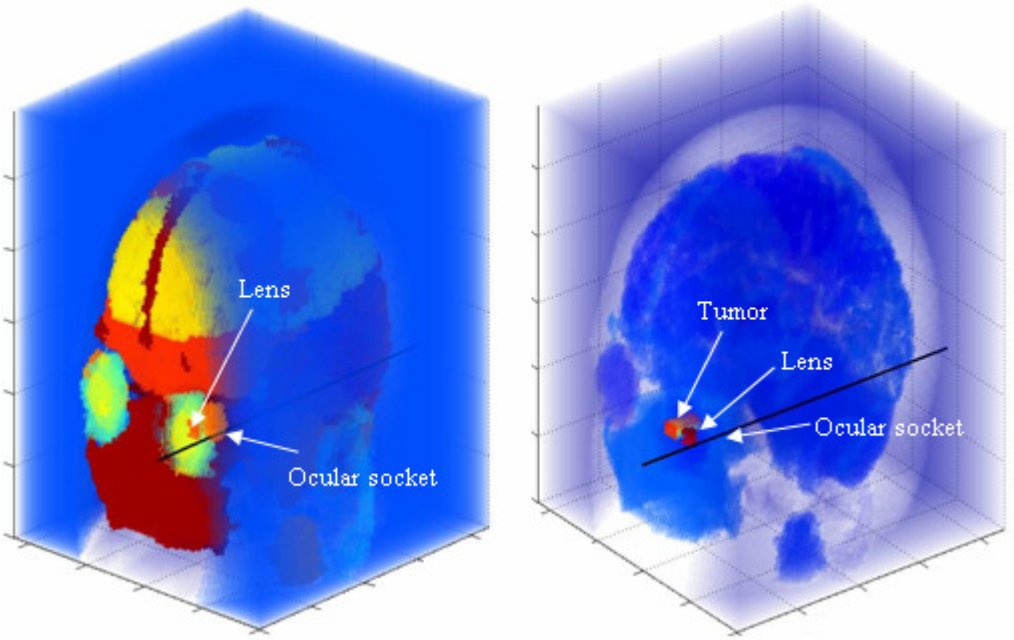


**Fig. 28**: Ocular socket worst case: proton beam into the ocular socket nearest the lens (left) and missing both the tumor and lens (right)

**Table 6**: Dose deposition during the ocular socket worst case scenario

| **Modified Zubal phantom** | | |
|---|---|---|
| **Dose Volume** | **Dose per Fraction (Gy)** | **Total Dose (Gy)** |
| Cornea | 0.00 | 0.00 |
| Anterior/Vitreous humor | 0.0001 | 0.0002 |
| Lens | 0.0003 | 0.0012 |
| Optic Nerve | 0.00 | 0.00 |
| Eye Wall | 0.0007 | 0.0029 |
| Tumor | 0.00 | 0.00 |

As expected, doses to all tissues of the eye were very low indicating that little or no detrimental effects would occur within the eye post irradiation.

Neutron absorbed-dose values were also calculated for this simulation. As expected, neutron absorbed-dose distributions agreed with values obtained during the previous two cases.

*Error Discussion*

To ensure the precision of the results obtained for all simulations, the MCNPX code includes ten standard statistical tests. All simulations performed during this research earned passing marks. Two of the tests are discussed here.

Printed out with each tally bin is the tally mean related to fluctuations in the number of particles simulated. These errors are not reliable (hence neither is the tally itself) unless the error is low. Only random fluctuations in tally values with increased particle histories should be observed, which was true for all simulations (Hughes et al. 2002).

Another statistical measure is the relative error ($R$) which is the estimated relative error defined as one estimated standard deviation of the mean divided by the estimated mean. The relative error relates the tally mean with the overall uncertainty. In MCNPX, the quantities required for this error estimate are computed after each complete history, thus accounting for "the fact that the various contributions to a tally from the same history are correlated" (Shultis and Faw 2006). Therefore, by using the estimated relative error one can form confidence intervals about the estimated mean; thus allowing statements about the true results to be made. Guidelines for interpreting the quality of the confidence interval for various values of $R$ are listed in Table 7 (Shultis and Faw 2006).

**Table 7**. Interpretation of the relative error R (Shultis and Faw 2006)

| Simulation R Value | Quality of Talley |
|---|---|
| > 0.5 | Meaningless |
| 0.2 to 0.5 | Factor of a few |
| < 0.1 | Reliable (except for point/ring detectors) |
| < 0.05 | Reliable even for point/ring detectors |

The relative errors for all cases were below 0.05 indicating reliable results. Furthermore, all simulations attained excellent statistics in the remaining eight statistical indices performed by MCNPX.

# CHAPTER IV

# CONCLUSIONS

*Summary*

The primary objective of this research was to develop a complex MCNPX model of the human head to predict absorbed dose distributions and neutron absorbed-dose values during proton therapy of ocular tumors. Absorbed dose distributions using the complex geometry were compared to a simple MCNPX model of the human eye developed by Oertli (2006). Dose calculations included contributions due to proton and secondary interactions, multiple coulombic energy scattering, elastic and inelastic scattering, and non-elastic nuclear reactions. Once MCNPX was properly benchmarked, the proton beam and MCNPX models were combined to predict dose distributions for three treatment scenarios. First, an ideal treatment scenario was modeled where the dose was maximized to the tumor volume and minimized elsewhere. The second situation, a worst case scenario, mimicked a patient starring directly into the treatment beam during therapy. During the third simulation the treatment beam was aimed into the bone surrounding the eye socket to estimate the dose to the vital regions of the eye due to scattering. Dose distributions for all cases were calculated throughout the vital tissues of the eye. Dose distributions observed for all three cases were as expected. Superior dose distributions were observed with the complex geometry for all tissues of the phantom and the tumor volume. During the ideal case simulation, therapeutic doses were achieved within the tumor volume while sparing all vital tissues of the eye. The worst case scenario in which the proton beam was directed into the lens of the eye yielded expected

results as well. The lens of the eye received doses above recommended limits indicating that detrimental effects are likely post irradiation. The worst case simulation in which the proton beam was directed into the ocular socket also produced anticipated results. Minimal doses due to scattering were observed in all tissues of the head and eye.

*Eye Model Conclusions*

Although difficult to model, complex geometries produced superior results during proton therapy simulations. Great detail incorporated into the modified Zubal phantom allows simulations to model many cancerous tumors. The eye phantom defined by Oertli (2006) will not allow for certain tumors to be modeled due to the simplicities of the model. Although a simplified tumor was modeled in the complex geometry, a large tumor was simulated. Simulating a large tumor in a voxel-based geometry produced a dose distribution across a large region of the eye. The distribution obtained allows dose estimates for complex tumors to be made. The densities of the tumor and tissues surrounding the tumor differ slightly; therefore, the dose profile will be similar in all tissues. However, simulating a dose distribution closer to the actual distribution is relatively simple using the Zubal phantom. Changing the density of selected voxels to match the density of the surrounding aqueous humor would modify the shape and size of the tumor; thus resulting in a more complex tumor. Further modifications would be required for proper simulation if the size and shape of the tumor is changed. For example, the energy spectrum produced by the modulator would need to be adjusted to maximize dose within the complex tumor volume and minimize it elsewhere. These two modifications would produce a reliable dose distribution through a complex tumor.

Additionally, a shape modifier (collimator) could be simulated between the proton beam the patient. The shape modifier would collimate the beam into the shape of the tumor further limiting the dose to healthy tissues surround the lesion.

Furthermore, tissues outside the eye including the brain, sinuses, skeletal bone and skin that were neglected in the simplified model were included in the modified Zubal phantom; thus allowing for dose deposition calculations to be made to regions outside the eye. The complex geometry predicts doses to 29 critical structures within the eye and head while the simplified model infers dose to adjacent organs by adjusting the penetration depth of the proton beam. This method is not adequate in all cases. The structure of the ocular socket for example, limits treatment angles of the proton beam. If the treatment angle is too great, the ocular socket protruding from below or above the eye socket will interfere with the treatment. Because the simplified phantom does not model such structures, it was not possible estimate doses to tissues surrounding the eye. Understanding doses outside the eye is critical when designing treatments for cancer patients.

Although very complex, more detail can be added within the eye of the modified Zubal phantom. For example, cilliary bodies and the iris surrounding the lens are areas where cancerous growth can occur. With the Zubal phantom it is possible to place a tumor in the general vicinity of the iris; however, it is not possible to simulate these types of tumors and their treatments in their exact location. Additionally, greater resolution could be obtained by reducing voxel dimensions further. The current voxel size is 2.2 x 2.2 x 1.4 mm. Reducing the voxel size by half would increase the resolution of the

organs within the head and eye. Doses to the sclera, choroid and retina might then be obtainable.

*Simulation Conclusions*

For all cases the modified Zubal phantom produced superior results in comparison to the simplified model. Dose distributions through both tumor and lens were able to be produced for the ideal case; thus ensuring that the Bragg peak occurred within the tumor volume and minimized doses to healthy tissues. Additionally, a dose distribution through the lens of the eye was produced for the case simulating a patient gazing into the treatment beam. This dose distribution allows one to estimate the severity to which the lens was irradiated. Although dose deposition within the eye was minimal during the worst case in which the ocular socket was the target, such a simulation is impossible with the simplified model. This research shows that, for all simulations modeled herein, a complex voxel base phantom produced higher quality results when compared to a simplified model.

# REFERENCES

Agosteo S, Birattari C, Caravaggio M, SilariMand G. Secondary neutron and photon dose in proton therapy. Radiother Oncol 11(48):293–305; 1998.

Constable I., Koehler A., Experimental ocular irradiation with accelerated protons. Invest. Opthalmol. Vis. Sci. 47(11): 280–287; 1974.

Cirrone P., Cuttone G., Lojacono P. A., Lo Nigro S. Mongelli V., Patti I. V., Privitera G., Raffaele L., Rifuggiato D., Sabini M. G., Salamone V., Spatola C., Valastro L. M. A 62 MeV proton beam for the treatment of ocular melanoma at Laboratori Nazionali del Sud-INFN. IEEE Trans. Nucl. Sci. 51(3): 860–865; 2004.

Evans J., Li C. Modified Zubal phantom input deck. Department of Mechanical Engineering, The Ohio State University; 2007.

Gargoundas E. S., Proton beam irradiation of uveal melanomas: The first 30 years – The Weisenfield Lecture. Invest. Opthalmol. Vis. Sci. 13(4): 4666–4673; 2006.

Hughes G., Chadwick M., Egdorf H., Little R., Macfarlane R., Mashink S., Pitcher E., Prael R., Sierk A., Waters L., While M., Young P., Gallmeier F., Snow E., Corzine R. Status of the MCNPX transport code. Los Alamos National Laboratory Report LA-UR-00–4942; 2000.

Hughes G., Chadwick M., Egdorf H., Little R., Macfarlane R., Mashink S., Pitcher E., Prael R., Sierk A., Waters L., While M., Young P., Gallmeier F., Snow E., Corzine R. MCNPX user manual. Los Alamos National Laboratory Report LA-UR-02–2607; 2002.

International Atomic Energy Agency. Radiation protection in nuclear medicine Available at: rpop.iaea.org/.../Content/Documents/TrainingNuclearMedicine/Lectures/RPNM_Part01_biological_effects_WEB.ppt. Accessed 17 March 2007.

Levin WP, Kooy H, Loeffler JS, Delaney TF. Proton beam therapy. Br J Cancer 93(8):849–854; 2005.

Metz, J. Reduce normal tissue toxicity with proton therapy. Available at: http://www.oncolink.org/treatment/article.cfm?c=9&s=70&id=211. Accessed 13 March 2006.

Newhauser W, Koch N, Hummel S, Ziegler M, Titt U. Monte Carlo simulations of a nozzle for the treatment of ocular tumours with high-energy proton beams. Phys Med Biol 50:5229–5249; 2005.

Oertli, D. Proton dose assessment to the human eye using Monte Carlo N-particle Transport Code (MCNPX). M.S. Thesis. Texas A&M University; 2006.

Paganetti H. Calculation of the spatial variation of relative biological effectiveness in a therapeutic proton field for eye treatment. Phys Med Biol 43:2147–2157; 1998.

Paganetti H, Jiang H, Lee SY, Kooy HM. Monte Carlo simulations for nozzle design, commissioning and quality assurance for a proton radiation therapy facility. Med Phys 31:2107–2118; 2004.

Pasciak, A. Various MATLAB routines. Texas A&M University; 2007.

Raju, M.R. Heavy particle radiotherapy. Los Angeles, California: Academic Press; 1980.

Romero JL. Patient positioning for proton therapy using a proton range telescope. Nucl Instrum Methods A 356:558–565; 1995.

Siebers J. Application of Monte Carlo to proton therapy radiation therapy. Proceedings from Advanced Monte Carlo for Radiation Physics, Particle Transport Simulations, and Applications. Lisbon: Nuclear Energy Agency; (New York: Springer) pp 1051–1056; 2000.

Simonova G, Novotny J, Liscak R, Pilbauer J. Leksell gamma knife treatment of uveal melanoma. J Neurosurg 97:635-639; 2002.

Shultis J, Faw R. An MCNP primer. Available at: http://ww2.mne.ksu.edu/~jks/MCNPprmr.pdf. Accessed 3 January 2006.

Smith A. Proton therapy. Phys Med Biol 51:R491–R504; 2006.

Turesson I., Johansson K-A., Mattsson S. The potential of proton and light ion beams in radiotherapy. Acta Oncologica 42:107–114; 2003.

Urie M, Sisterson J, Koehler A, Goitein M, Zoesman J. Proton beam penumbra: effects of separation between patient and beam modifying devices. Med Phys 13:734–741; 1986.

Verhaegen F, Palmans H. A systematic Monte Carlo study of secondary electron fluence perturbation in clinical proton beams (70–250 MeV) for cylindrical and spherical ion chambers. Med Phys 28:2088–2095; 2001.

Zubal, G. The Zubal phantom. Available at: http://noodle.med.yale.edu/zubal/info.htm. accessed 12 April 2007

*Supplemental Sources – Used for background knowledge*

Hendricks, McKinney JS, Waters GW, Roberts LS, Egdorf TL, Finch HW, Trellue JP, Pitcher HR, Mayo EJ, Swinhoe DR, Tobin MT, Durkee SJ, Gallmeier JW, David FX, Hamilton JC, Lebenhaft WB, J. MCNPX extensions version 2.5.0. Los Alamos National Laboratory Report LA-UR-04-0570; 2004.

Hughes G, Prael R, Little R. MCNPX—the LAHET/MCNP code merger technical report LA-UR-97-4891 Los Alamos National Laboratory, 1997.

Medin J, Andreo P. Monte Carlo calculated stopping-power ratios, water/air, for clinical proton dosimetry (50–250 MeV). Phys Med Biol 42:89–105; 1997.

Munzenrider J, Verhey LJ, Gragoudas ES, Seddon JM, Urie M, Gentry R, Birnbaum S, Ruotolo DM, Crowell C, McManus P. Conservative treatment of uveal melanoma: local recurrence after proton beam therapy. Int J Radiat Oncol Biol Phys 17:493–8; 1989.

Newhauser WD, Titt U, Dexheimer D, Yan X, Nill S. Neutron shielding verification measurements and simulations for a 235-MeV proton therapy center. Nucl Instrum Methods A. 476:80–84; 1989.

Paganetti H. Calculation of the spatial variation of relative biological effectiveness in a therapeutic proton field for eye treatment. Phys Med Biol 43:2147–2157; 1998.

Paganetti H. Monte Carlo method to study the proton fluence for treatment planning. Med Phys 25:2370–2375; 1998.

Polf JC, Newhauser WD. Effect of range modulation on the neutron dose equivalent around a passive scattering proton therapy treatment nozzle. Phys Med Biol 50:3859–3873; 2005.

Sakae T, Nohtomi A, Maruhashi A, Sato M, Terunuma T, Kohno R, Akine Y, Hayakawa Y, Koike Y. Multi-layer energy filter for realizing conformal irradiation in charged particle therapy. Med Phys 27:368–373; 2000.

Schneider U, Agosteo S, Pedroni E, Besserer J. Secondary neutron dose during proton therapy using spot scanning. Int J Radiat Oncol Biol Phys 53:244–251; 2002.

Schulte RW, Bashkirov V, Loss-Klock MC, Li T, Wroe AJ, Evseev I, Williams DC, Satogata T. Density resolution of proton computed tomography. Med Phys 32:1035–1046; 2005.

Suit HD. Protons to replace photons in external beam radiation therapy? Clin Oncol 15:S29-S31; 2002.

Tourovsky A, Lomax AJ, Schneider U, Pedroni E. Monte Carlo dose calculations for spot scanned proton therapy. Phys Med Biol 50:971–981; 2005.

Wroe AJ, Cornelius IM, Rosenfeld AB. The role of nonelastic reactions in absorbed dose distributions from therapeutic proton beams in different medium. Med Phys 32:37–41; 2005.

Zaidi H. Therapeutic Applications of Monte Carlo Calculations in Nuclear Medicine. London: IOP Publishing Ltd; 2003.

# APPENDIX A

## **MATLAB routines** (Pasciak 2007)

*Routine to read MCNPX matrix into3-dimensional MATLAB matrix*

```
clc; clear all;
filename = 'phan';
fid = fopen(filename, 'r');

VoxMap = zeros(85, 109, 119);
INDEX_X = 1;
INDEX_Y = 1;
INDEX_Z = 1;

INDEX_X_MAX = 85;
INDEX_Y_MAX = 109;
INDEX_Z_MAX = 120;

myline = fgetl(fid);

i = 0;
current_line = 1;
while 1
    tempchar = '';
    charcnt = 1;
    for i = 1:length(myline)
        tempchar;
        if(myline(i) ~= ' ')
            tempchar(charcnt) = myline(i);
            charcnt = charcnt + 1;
        end
        if((myline(i) == ' ') | (i == length(myline)))
            if(charcnt ~= 1)

                prevchar = tempchar;
                if(prevchar(end) == 'r')
                    numentries = str2num(prevchar(1:(end-1)));
                    entry = str2num(olderchar);
                else
                    numentries = 1;
                    entry = str2num(prevchar);
                end
                olderchar = prevchar;

                for jp = 1:numentries
                    if(INDEX_X > INDEX_X_MAX)
                        INDEX_X = 1;
                        INDEX_Y = INDEX_Y + 1;
                    end
                    if(INDEX_Y > INDEX_Y_MAX)
                        INDEX_Z = INDEX_Z + 1;
                        INDEX_X = 1;
                        INDEX_Y = 1;
```

```
                    end

                   % [INDEX_X INDEX_Y INDEX_Z entry]
                    VoxMap(INDEX_X, INDEX_Y, INDEX_Z) = entry;
                    INDEX_X = INDEX_X + 1;
                end

                tempchar = '';
                charcnt = 1;
            end
        end
    end
    myline = fgetl(fid);
    current_line = current_line + 1;
    if(mod(current_line,100) == 0)
        current_line
    end

    if ~ischar(myline), break, end

end
fclose(fid)
```

*Routine to plot 3-dimensional MATLAB matrix*

```
%%%%%%%%%%%%%%%%%%%%%%%%%%%%%%%%%%%%%%%%%%%%%%%%%%%%%%%%%%%%%%%%%%%%%%%%
%%%%%  START EDITING %%%%%%%%%%%%%%%%%%%%%%%%%%%%%%%%%%%%%%%%%%%%%%%%%%
%%%%%%%%%%%%%%%%%%%%%%%%%%%%%%%%%%%%%%%%%%%%%%%%%%%%%%%%%%%%%%%%%%%%%%%%
%
% Plot a line over the phantom
plotline = 1;            % set to 0 for no line, 1 for a line
direction = [0 1 0];     % unit vector direction (X,Y,Z)
start_coor = [-2.9 -10.96 83.77];  % where to start the line (in cm)
(X, Y, Z)
line_width = 2;

z_start_vox =  772;  %Z value at the bottom of the voxel map (in mm)

phantom_opacity = .95;  %the opacity of the voxel phantom
size_x = 2.2;  %size of X voxel in mm
size_y = 2.2;  %size of Y voxel in mm
size_z = 1.4;  %size of Z voxel in mm

Xmax = 85;
Ymax = 109;
Zmax = 120;

Xrange = [1:85];   %max 85
Yrange = [23:109];  %max 109
Zrange = [1:120];  %max 120

%%%%%%%%%%%%%%%%%%%%%%%%%%%%%%%%%%%%%%%%%%%%%%%%%%%%%%%%%%%%%%%%%%%%%%%%
%%%%%  STOP EDITING %%%%%%%%%%%%%%%%%%%%%%%%%%%%%%%%%%%%%%%%%%%%%%%%%%%%
%%%%%%%%%%%%%%%%%%%%%%%%%%%%%%%%%%%%%%%%%%%%%%%%%%%%%%%%%%%%%%%%%%%%%%%%


start_coor = start_coor .* 10;
%axis([((min(Xrange) - .5) .* size_x) ((max(Xrange) - .5) .* size_x)
((min(Yrange) - .5) .* size_y) ((max(Yrange) - .5) .* size_y)
((min(Zrange) - .5) .* size_z) ((max(Zrange) - .5) .* size_z)])
hold on
close all; clc; hold off;
h = vol3d('cdata',VoxMap(Xrange, Yrange, Zrange),'texture','2D');
view(3);
vol3d(h);
grid;
alphamap(alphamap .* phantom_opacity);  %Change opacity
xlabel('Y Axis');
ylabel('X Axis');
zlabel('Z Axis');
if (plotline == 1)
    hold on;
    xvst = (((start_coor(1) ./ size_x)) - (min(Xrange) - 1)) + (Xmax ./
2);
    yvst = (((start_coor(2) ./ size_y)) - (min(Yrange) - 1)) + (Ymax ./
2);
    zvst = (((start_coor(3) ./ size_z)) - (min(Zrange) - 1)) -
(z_start_vox ./ size_z);
    T = [0:100];
```

```
    plot3((T .* direction(2)) + yvst, (T .* direction(1)) + xvst,  (T
.* direction(3)) + zvst, 'k-', 'LineWidth', line_width );
end

colorbar
vol3dtool

%%%%%%%%%%%%%%%%%%%%%
% tempVmap = VoxMap;
% pcolor(VoxMap(:,:,Z))
% VoxMap(X,Y,Z) = #
```

*Routine to write MATLAB code back to MCNPX matrix format*

```
filename = 'filename';
%voxel map must be named "VoxMap"
fid = fopen(filename, 'w');

INDEX_X_MAX = 85;
INDEX_Y_MAX = 109;
INDEX_Z_MAX = 120;


%%%%%%%%%%%%%%%%%%%%%%%%%%%%%%%%
%%%%%%%%%%%%%%%%%%%%%%%%%%%%%%%%


INDEX_X = 1;
INDEX_Y = 1;
INDEX_Z = 1;

startline = '     ';
stop = 0;
while(INDEX_Z <= INDEX_Z_MAX)
    while(length(startline) < 75)

        if(INDEX_X > INDEX_X_MAX)
            INDEX_X = 1;
            INDEX_Y = INDEX_Y + 1;
        end
        if(INDEX_Y > INDEX_Y_MAX)
            INDEX_Z = INDEX_Z + 1;
            INDEX_X = 1;
            INDEX_Y = 1;
        end
        if(INDEX_Z == (INDEX_Z_MAX + 1))
            break;
        end

        % [INDEX_X INDEX_Y INDEX_Z entry]
        startline = cat(2, startline, num2str(VoxMap(INDEX_X, INDEX_Y,
INDEX_Z)), ' ');
        INDEX_X = INDEX_X + 1;
    end
    while(length(startline) < 80)
        startline = cat(2, startline, ' ');
    end
    fprintf(fid, '%s\n', startline);
    startline = '     ';
end

fclose(fid)
```

## APPENDIX B

*MCNPX Output deck – Ideal Case Scenario– tally change from h to n for the neutron case*
*For the worst case scenario (lens) the source location was changed to (-3.74 -10.1 83.85) (All else the same – tally change from h to n for the neutron case)*
*For the worst case scenario (ocular socket) the source location was changed to (-4.96 -8.9 83.43) (All else the same – tally change from h to n for the neutron case)*

```
1mcnpx    version 2.5.0 ld=Mon Mar 21 08:00:00 MST 2005               04/07/07 19:49:22
 ******************************************************************************   probid =   04/07/07 19:49:22
 i=icwt4 o=icwt4o


 warning.  universe map (print table 128) disabled.
 ************************************************
 *                                              *
 *            Copyright Notice for MCNPX        *
 *                                              *
 * This program was prepared by the Regents of the   *
 * University of California at Los Alamos National   *
 * Laboratory (the University) under contract number *
 * W-7405-ENG-36 with the U.S. Department of Energy  *
 * (DOE).  The University has certain rights in the  *
 * program pursuant to the contract and the program  *
 * should not be copied or distributed outside your  *
 * organization.   All rights in the program are     *
 * reserved by the DOE and the University.  Neither  *
 * the U.S. Government nor the University makes any  *
 * warranty, express or implied, or assumes any      *
 * liability or responsibility for the use of this   *
 * software.                                         *
 *                                              *
 ************************************************
    1-       Modified Zubal head phantom
    2-       c Modified Zubal phantom Input Deck by Jeff Evans. Revisions by Chenguan Li.
    3-       c   Department of Mechanical Engineering, The Ohio State University, Columbus 43
    4-       c
    5-       c Based on the Zubal phantom. ref -
    6-       c   I. G. Zubal, C. R. Harrell, E. O. Smith, and A. L. Smith,
    7-       c   "Two dedicated software, voxel-based, anthropomorphic (torso and head) phant
    8-       c   in Proceedings of the International Workshop, National Radiological Protecti
    9-       c   Chilton, UK, on 6 and 7 July 1995, edited by P. J. Dimbylow (NRPB, Chilton,
   10-       c
```

```
   11-       c This geometric model has been used in:  J.F. Evans, T. E. Blue, N. Gupta,
   12-       c   "Absorbed dose estimates to structures of the brain and head using a high-re
   13-       c   voxel-based head phantom." Med Phys. 2001 May;28(5):780-6.
   14-       c
   15-       c Most of the head is 85 x 109 x 120 lattice of voxels, where each voxel is 2.2
   16-       c   29 critical structures of the head are identified by their individual univer
   17-       c   attached to a simplistic model of the neck and torso.
   18-       c
   19-       c Other citations in this input deck:
   20-       c   J. E. Woollard, T. E. Blue, N. Gupta, and R. A. Gahbauer, "Development and a
   21-       c   neutron field optimization parameters for an accelerator-based neutron sourc
   22-       c   neutron capture therapy," Nucl. Technol. 115, 100-113 (1996).
   23-       c
   24-       c   ICRU 46, "Photon, electron, proton, and neutron interaction data for body ti
   25-       c   International Commission on Radiation Units and Measurements, Bethesda, MD,
   26-       c
   27-       c Begin MCNP input deck.
   28-         998 0 -2 1  -4 3  -6  5             fill=999 (-8.91 -13.42 77.2)
   29-         999 0 -8 7 -10 9 -12 11 u=999 lat=1 fill=0:84 0:108 0:119
*****************************************************************************************************************************
                                                  Voxel matrix omitted due to length.
*****************************************************************************************************************************
41271-           1 12 -1.09 -8 7 -10 9 -12 11    vol=232.159 u=1  $ skin
41272-           2 like 1 but mat=4  rho=-1.007  vol=214.027 u=2  $ cerebral fluid
41273-           3 like 1 but mat=14 rho=-0.95   vol=551.058 u=3  $ fat
41274-           4 like 1 but mat=8  rho=-1.61   vol=557.461 u=4  $ skeletal bone
41275-           5 like 1 but mat=7  rho=-1.05   vol=409.840 u=5  $ skeletal muscle
41276-           6 like 1 but mat=3  rho=-1.043  vol=246.965 u=6  $ white matter (left)
41277-           7 like 1 but mat=3  rho=-1.043  vol=245.413 u=7  $ white matter (right)
41278-           8 like 1 but mat=2  rho=-1.039  vol=120.050 u=8  $ temporal lobe (left)
41279-           9 like 1 but mat=2  rho=-1.039  vol=121.697 u=9  $ temporal lobe (right)
41280-          10 like 1 but mat=11 rho=-1.038  vol=2.96789 u=10 $ spinal cord
41281-          20 like 1 but mat=1  rho=-1      vol=9640.50 u=20 $ water (outside phantom)
41282-          26 like 1 but mat=10 rho=-1.18   vol=7.31808 u=26 $ bone marrow
41283-          30 like 1 but mat=9  rho=-1.10   vol=58.2397 u=30 $ cartilage
41284-          40 like 1 but mat=2  rho=-1.039  vol=4.65511 u=40 $ internal capsule (left)
41285-          41 like 1 but mat=2  rho=-1.039  vol=4.39085 u=41 $ internal capsule (right)
41286-          42 like 1 but mat=2  rho=-1.039  vol=1.00962 u=42 $ septum pellucidium
41287-          43 like 1 but mat=2  rho=-1.039  vol=6.24747 u=43 $ thalamus (left)
41288-          44 like 1 but mat=2  rho=-1.039  vol=6.13228 u=44 $ thalamus (right)
41289-          45 like 1 but mat=5  rho=-1.076  vol=7.27742 u=45 $ eyeball (left)
41290-          46 like 1 but mat=5  rho=-1.076  vol=6.35589 u=46 $ eyeball (right)
41291-          47 like 1 but mat=2  rho=-1.039  vol=11.2685 u=47 $ corpus callosum
41292-          48 like 1 but mat=2  rho=-1.039  vol=2.53422 u=48 $ motor cortex (left)
41293-          49 like 1 but mat=2  rho=-1.039  vol=3.45576 u=49 $ motor cortex (right)
41294-          50 like 1 but mat=7  rho=-1.05   vol=4.04527 u=50 $ falx cerebri
41295-          51 like 1 but mat=2  rho=-1.039  vol=63.1523 u=51 $ parietal lobe (left)
```

```
41296-          52 like 1 but mat=2  rho=-1.039  vol=63.2540 u=52 $ parietal lobe (right)
41297-          55 like 1 but mat=2  rho=-1.039  vol=2.14122 u=55 $ amygdala (left)
41298-          56 like 1 but mat=2  rho=-1.039  vol=1.86340 u=56 $ amygdala (right)
41299-          57 like 1 but mat=5  rho=-1.009  vol=6.67436 u=57 $ eye (left)
41300-          58 like 1 but mat=5  rho=-1.009  vol=6.35589 u=58 $ eye (right)
41301-          59 like 1 but mat=2  rho=-1.039  vol=2.00570 u=59 $ globus pallidus (left)
41302-          60 like 1 but mat=2  rho=-1.039  vol=1.91761 u=60 $ globus pallidus (right)
41303-          61 like 1 but mat=6  rho=-1.07   vol=.203280 u=61 $ lens (left)
41304-          63 like 1 but mat=2  rho=-1.039  vol=26.8872 u=63 $ prefrontal lobe (left)
41305-          64 like 1 but mat=2  rho=-1.039  vol=28.0933 u=64 $ prefrontal lobe (right)
41306-          72 like 1 but mat=7  rho=-1.05   vol=18.9389 u=72 $ parotid gland (left)
41307-          73 like 1 but mat=7  rho=-1.05   vol=14.0195 u=73 $ parotid gland (right)
41308-          74 like 1 but mat=7  rho=-1.05   vol=1.07738 u=74 $ lacrimal gland (left)
41309-          75 like 1 but mat=7  rho=-1.05   vol=1.39586 u=75 $ lacrimal gland (right)
41310-          76 like 1 but mat=3  rho=-1.043  vol=15.5645 u=76 $ cerebellum (white matter)
41311-          77 like 1 but mat=2  rho=-1.039  vol=147.514 u=77 $ cerebellum (cortex)
41312-          80 like 1 but mat=2  rho=-1.039  vol=4.41795 u=80 $ medulla oblongata
41313-          81 like 1 but mat=2  rho=-1.039  vol=59.0732 u=81 $ frontal lobe (left)
41314-          82 like 1 but mat=2  rho=-1.039  vol=58.6869 u=82 $ frontal lobe (right)
41315-          83 like 1 but mat=2  rho=-1.039  vol=23.3975 u=83 $ pons
41316-          84 like 1 but mat=2  rho=-1.039  vol=37.0105 u=84 $ occipital lobe (left)
41317-          85 like 1 but mat=2  rho=-1.039  vol=36.0144 u=85 $ occipital lobe (right)
41318-          86 like 1 but mat=2  rho=-1.039  vol=3.37445 u=86 $ hippocampus (left)
41319-          87 like 1 but mat=2  rho=-1.039  vol=3.89620 u=87 $ hippocampus (right)
41320-          88 like 1 but mat=7  rho=-1.066  vol=.128744 u=88 $ pituitary gland
41321-          89 like 1 but mat=2  rho=-1.039  vol=.230384 u=89 $ uncus (left)
41322-          90 like 1 but mat=2  rho=-1.039  vol=.345576 u=90 $ uncus (right)
41323-          91 like 1 but mat=2  rho=-1.039  vol=5.10910 u=91 $ caudate nucleus (left)
41324-          92 like 1 but mat=2  rho=-1.039  vol=5.21074 u=92 $ caudate nucleus (right)
41325-          93 like 1 but mat=2  rho=-1.039  vol=7.03349 u=93 $ insula cortex (left)
41326-          94 like 1 but mat=2  rho=-1.039  vol=6.75567 u=94 $ insula cortex (right)
41327-          95 like 1 but mat=1  rho=-0.0012 vol=193.299 u=95 $ sinuses
41328-          96 like 1 but mat=2  rho=-1.039  vol=4.74998 u=96 $ putamen (left)
41329-          97 like 1 but mat=2  rho=-1.039  vol=5.18364 u=97 $ putamen (right)
41330-          98 like 1 but mat=2  rho=-1.039  vol=.718256 u=98 $ optic nerve (left)
41331-          99 like 1 but mat=2  rho=-1.039  vol=.542074 u=99 $ optic nerve (right)
41332-         141 11 -1.038 -38  -5  39             vol=4.18     $spinal cord
41333-         142  4 -1.007 -40  38  -5  39         vol=9.22     $CSF_spinal
41334-         143  8 -1.61  -41  40  -5  39         vol=68.53    $skeleton_spine
41335-         150  8 -1.61  -49  50 -46  -5  51     vol=58.1     $skeleton_mandible_1
41336-         151  8 -1.61  -49  52  -9  46  -5  51 vol=24.07    $skeleton_mandible_2
41337-         153 13 -1.05  -54  55 -59 (((56:-63) 60 -64 (58:-57)):(57 -58 61 -62))
41338-                                             vol=20.03    $thyroid
41339-         154  7 -1.05  -65 -66  -5  67 (41:5:66:-67) #150 #151 vol=276.9  $head_face
41340-         156  7 -1.05  -68  66  -5  67 (41:5:-66:-67)          vol=28.3   $head_back_2
41341-         157  7 -1.05  -70  68  66  -5 67                      vol=1.181  $head_back_3
41342-         158  7 -1.05  -70 -67  39 (41:67:-39) (54:-55:-57:58:59:-61:62)
```

```
41343-                    (54:-55:(-56 63):57:59:-60:64) (54:-55:(-56 63):-58:59:-60:64)
41344-                                                   vol=472.1   $head_neck
41345-        161 12 -1.09  -72  65 -66  -5  67          vol=15.08   $skin_face_1
41346-        162 12 -1.09  -72  68 -73  66  -5  67  70 vol=2.0     $skin_face_2
41347-        163 12 -1.09  -72  74 -73 -67  64          vol=20.31   $skin_face_3
41348-        164 12 -1.09  -74  70 -67  39              vol=38.619  $skin_neck
41349-        165 12 -1.09  -75  68  73  -5  67  70      vol=2.26    $skin_back_1
41350-        166 12 -1.09  -74  70  75  73  -5  67      vol=1.353   $skin_back_2
41351-        167  7 -1.05  -79 -39  11                  vol=43982.3 $trunk
41352-        168 12 -1.09  -81  79 -39  11              vol=1328.27 $trunk_skin
41353-        200  1 -1 -99   5 #998                          $water (outside phantom)
41354-        201  1 -1 -99  -5  39 (72:73:5:-64) (74:67:-39) (75:-73:5:-67)
41355-                    (74:-75:-73:-67)                    $water (outside phantom)
41356-        202  1 -1 -99 -39 (81:39:-11)                  $water (outside phantom)
41357-        205 like 1 but mat=6  rho=-1.07   vol=.006776 u=205 $ TUMOR
41358-        206 like 1 but mat=6  rho=-1.07   vol=.006776 u=206 $ TUMOR
41359-        207 like 1 but mat=6  rho=-1.07   vol=.006776 u=207 $ TUMOR
41360-        208 like 1 but mat=6  rho=-1.07   vol=.006776 u=208 $ TUMOR
41361-        209 like 1 but mat=6  rho=-1.07   vol=.006776 u=209 $ TUMOR
41362-        210 like 1 but mat=6  rho=-1.07   vol=.006776 u=210 $ TUMOR
41363-        211 like 1 but mat=6  rho=-1.07   vol=.006776 u=211 $ TUMOR
41364-        212 like 1 but mat=6  rho=-1.07   vol=.006776 u=212 $ TUMOR
41365-        213 like 1 but mat=6  rho=-1.07   vol=.006776 u=213 $ TUMOR
41366-        214 like 1 but mat=6  rho=-1.07   vol=.006776 u=214 $ TUMOR
41367-        215 like 1 but mat=6  rho=-1.07   vol=.006776 u=215 $ TUMOR
41368-        216 like 1 but mat=6  rho=-1.07   vol=.006776 u=216 $ TUMOR
41369-        217 like 1 but mat=5  rho=-1.009  vol=.006776 u=217 $ Eye (BT)
41370-        218 like 1 but mat=5  rho=-1.009  vol=.006776 u=218 $ Eye (BT)
41371-        219 like 1 but mat=5  rho=-1.009  vol=.006776 u=219 $ Eye (BT)
41372-        220 like 1 but mat=5  rho=-1.009  vol=.006776 u=220 $ Eye (BT)
41373-        221 like 1 but mat=5  rho=-1.009  vol=.006776 u=221 $ Eye (BT)
41374-        222 like 1 but mat=5  rho=-1.009  vol=.006776 u=222 $ Eye (BT)
41375-        223 like 1 but mat=5  rho=-1.009  vol=.006776 u=223 $ Eye (LT)
41376-        224 like 1 but mat=6  rho=-1.07   vol=.006776 u=224 $ TUMOR
41377-        225 like 1 but mat=6  rho=-1.07   vol=.006776 u=225 $ TUMOR
41378-        226 like 1 but mat=6  rho=-1.07   vol=.006776 u=226 $ TUMOR
41379-        227 like 1 but mat=5  rho=-1.009  vol=.006776 u=227 $ Eye (RT)
41380-        228 like 1 but mat=5  rho=-1.009  vol=.006776 u=228 $ Eye (LT)
41381-        229 like 1 but mat=5  rho=-1.009  vol=.006776 u=229 $ Eye (RT)
41382-        230 like 1 but mat=5  rho=-1.009  vol=.006776 u=230 $ Eye (LT)
41383-        231 like 1 but mat=5  rho=-1.009  vol=.006776 u=231 $ Eye (RT)
41384-        232 like 1 but mat=5  rho=-1.009  vol=.006776 u=232 $ Eye (LT)
41385-        233 like 1 but mat=5  rho=-1.009  vol=.006776 u=233 $ Eye (RT)
41386-        234 like 1 but mat=5  rho=-1.009  vol=.006776 u=234 $ Eye (LT)
41387-        235 like 1 but mat=5  rho=-1.009  vol=.006776 u=235 $ Eye (RT)
41388-        236 like 1 but mat=14 rho=-0.95   vol=.006776 u=236 $ Fat (LT)
41389-        237 like 1 but mat=5  rho=-1.009  vol=.006776 u=237 $ Eye (RT)
```

```
41390-        238 like 1 but mat=14 rho=-0.95   vol=.006776 u=238 $ Fat (LT)
41391-        239 like 1 but mat=5  rho=-1.009  vol=.006776 u=239 $ Eye (RT)
41392-        240 like 1 but mat=14 rho=-0.95   vol=.006776 u=240 $ Fat (BT)
41393-        241 like 1 but mat=14 rho=-0.95   vol=.006776 u=241 $ Fat (BT)
41394-        242 like 1 but mat=5  rho=-1.009  vol=.006776 u=242 $ Eye (BT)
41395-        243 like 1 but mat=5  rho=-1.009  vol=.006776 u=243 $ Eye (BT)
41396-        244 like 1 but mat=5  rho=-1.009  vol=.006776 u=244 $ Eye (BT)
41397-        245 like 1 but mat=6  rho=-1.07   vol=.006776 u=245 $ TUMOR
41398-        246 like 1 but mat=6  rho=-1.07   vol=.006776 u=246 $ TUMOR
41399-        247 like 1 but mat=6  rho=-1.07   vol=.006776 u=247 $ TUMOR
41400-        248 like 1 but mat=6  rho=-1.07   vol=.006776 u=248 $ TUMOR
41401-        249 like 1 but mat=6  rho=-1.07   vol=.006776 u=249 $ TUMOR
41402-        250 like 1 but mat=6  rho=-1.07   vol=.006776 u=250 $ TUMOR
41403-        251 like 1 but mat=6  rho=-1.07   vol=.006776 u=251 $ TUMOR
41404-        252 like 1 but mat=6  rho=-1.07   vol=.006776 u=252 $ TUMOR
41405-        253 like 1 but mat=6  rho=-1.07   vol=.006776 u=253 $ TUMOR
41406-        254 like 1 but mat=6  rho=-1.07   vol=.006776 u=254 $ TUMOR
41407-        255 like 1 but mat=6  rho=-1.07   vol=.006776 u=255 $ TUMOR
41408-        256 like 1 but mat=6  rho=-1.07   vol=.006776 u=256 $ TUMOR
41409-        257 like 1 but mat=5  rho=-1.009  vol=.006776 u=257 $ Eye (BT)
41410-        258 like 1 but mat=5  rho=-1.009  vol=.006776 u=258 $ Eye (BT)
41411-        259 like 1 but mat=5  rho=-1.009  vol=.006776 u=259 $ Eye (BT)
41412-        260 like 1 but mat=5  rho=-1.009  vol=.006776 u=260 $ Eye (BT)
41413-        261 like 1 but mat=5  rho=-1.009  vol=.006776 u=261 $ Eye (BT)
41414-        262 like 1 but mat=5  rho=-1.009  vol=.006776 u=262 $ Eye (BT)
41415-        263 like 1 but mat=5  rho=-1.009  vol=.006776 u=263 $ Eye (LT)
41416-        264 like 1 but mat=6  rho=-1.07   vol=.006776 u=264 $ TUMOR
41417-        265 like 1 but mat=6  rho=-1.07   vol=.006776 u=265 $ TUMOR
41418-        266 like 1 but mat=6  rho=-1.07   vol=.006776 u=266 $ TUMOR
41419-        267 like 1 but mat=5  rho=-1.009  vol=.006776 u=267 $ Eye (RT)
41420-        268 like 1 but mat=5  rho=-1.009  vol=.006776 u=268 $ Eye (LT)
41421-        269 like 1 but mat=5  rho=-1.009  vol=.006776 u=269 $ Eye (RT)
41422-        270 like 1 but mat=5  rho=-1.009  vol=.006776 u=270 $ Eye (LT)
41423-        271 like 1 but mat=5  rho=-1.009  vol=.006776 u=271 $ Eye (RT)
41424-        272 like 1 but mat=5  rho=-1.009  vol=.006776 u=272 $ Eye (LT)
41425-        273 like 1 but mat=5  rho=-1.009  vol=.006776 u=273 $ Eye (RT)
41426-        274 like 1 but mat=5  rho=-1.076  vol=.006776 u=274 $ Eye Ball (LT)
41427-        275 like 1 but mat=5  rho=-1.009  vol=.006776 u=275 $ Eye (RT)
41428-        276 like 1 but mat=5  rho=-1.076  vol=.006776 u=276 $ Eye Ball (LT)
41429-        277 like 1 but mat=5  rho=-1.009  vol=.006776 u=277 $ Eye (RT)
41430-        278 like 1 but mat=2  rho=-1.039  vol=.006776 u=278 $ Optic Nerve (LT)
41431-        279 like 1 but mat=5  rho=-1.009  vol=.006776 u=279 $ Eye (RT)
41432-        280 like 1 but mat=2  rho=-1.039  vol=.006776 u=280 $ Optic Nerve (BT)
41433-        281 like 1 but mat=2  rho=-1.039  vol=.006776 u=281 $ Optic Nerve (BT)
41434-        282 like 1 but mat=14 rho=-0.95   vol=.006776 u=282 $ Fat (BT)
41435-        283 like 1 but mat=5  rho=-1.009  vol=.006776 u=283 $ Eye (BT)
41436-        284 like 1 but mat=5  rho=-1.076  vol=.006776 u=284 $ Eye Ball (BT)
```

```
41437-        285 like 1 but mat=6  rho=-1.07   vol=.006776 u=285 $ TUMOR
41438-        286 like 1 but mat=6  rho=-1.07   vol=.006776 u=286 $ TUMOR
41439-        287 like 1 but mat=6  rho=-1.07   vol=.006776 u=287 $ TUMOR
41440-        288 like 1 but mat=6  rho=-1.07   vol=.006776 u=288 $ TUMOR
41441-        289 like 1 but mat=6  rho=-1.07   vol=.006776 u=289 $ TUMOR
41442-        290 like 1 but mat=6  rho=-1.07   vol=.006776 u=290 $ TUMOR
41443-        291 like 1 but mat=6  rho=-1.07   vol=.006776 u=291 $ TUMOR
41444-        292 like 1 but mat=6  rho=-1.07   vol=.006776 u=292 $ TUMOR
41445-        293 like 1 but mat=6  rho=-1.07   vol=.006776 u=293 $ TUMOR
41446-        294 like 1 but mat=6  rho=-1.07   vol=.006776 u=294 $ TUMOR
41447-        295 like 1 but mat=6  rho=-1.07   vol=.006776 u=295 $ TUMOR
41448-        296 like 1 but mat=6  rho=-1.07   vol=.006776 u=296 $ TUMOR
41449-        297 like 1 but mat=5  rho=-1.009  vol=.006776 u=297 $ Eye (BT)
41450-        298 like 1 but mat=5  rho=-1.009  vol=.006776 u=298 $ Eye (BT)
41451-        299 like 1 but mat=5  rho=-1.009  vol=.006776 u=299 $ Eye (BT)
41452-        300 like 1 but mat=5  rho=-1.009  vol=.006776 u=300 $ Eye (BT)
41453-        301 like 1 but mat=5  rho=-1.009  vol=.006776 u=301 $ Eye (BT)
41454-        302 like 1 but mat=5  rho=-1.009  vol=.006776 u=302 $ Eye (BT)
41455-        303 like 1 but mat=5  rho=-1.076  vol=.006776 u=303 $ Eye Ball (LT)
41456-        304 like 1 but mat=6  rho=-1.07   vol=.006776 u=304 $ TUMOR
41457-        305 like 1 but mat=6  rho=-1.07   vol=.006776 u=305 $ TUMOR
41458-        306 like 1 but mat=6  rho=-1.07   vol=.006776 u=306 $ TUMOR
41459-        307 like 1 but mat=5  rho=-1.009  vol=.006776 u=307 $ Eye (RT)
41460-        308 like 1 but mat=5  rho=-1.009  vol=.006776 u=308 $ Eye (LT)
41461-        309 like 1 but mat=5  rho=-1.009  vol=.006776 u=309 $ Eye (RT)
41462-        310 like 1 but mat=5  rho=-1.009  vol=.006776 u=310 $ Eye (LT)
41463-        311 like 1 but mat=5  rho=-1.009  vol=.006776 u=311 $ Eye (RT)
41464-        312 like 1 but mat=5  rho=-1.009  vol=.006776 u=312 $ Eye (LT)
41465-        313 like 1 but mat=5  rho=-1.009  vol=.006776 u=313 $ Eye (RT)
41466-        314 like 1 but mat=5  rho=-1.009  vol=.006776 u=314 $ Eye (LT)
41467-        315 like 1 but mat=5  rho=-1.009  vol=.006776 u=315 $ Eye (RT)
41468-        316 like 1 but mat=14 rho=-0.95   vol=.006776 u=316 $ Fat (LT)
41469-        317 like 1 but mat=5  rho=-1.009  vol=.006776 u=317 $ Eye (RT)
41470-        318 like 1 but mat=14 rho=-0.95   vol=.006776 u=318 $ Fat (LT)
41471-        319 like 1 but mat=5  rho=-1.009  vol=.006776 u=319 $ Eye (RT)
41472-        320 like 1 but mat=2  rho=-1.039  vol=.006776 u=320 $ Optic Nerve (BT)
41473-        321 like 1 but mat=2  rho=-1.039  vol=.006776 u=321 $ Optic Nerve (BT)
41474-        322 like 1 but mat=14 rho=-0.95   vol=.006776 u=322 $ Fat (BT)
41475-        323 like 1 but mat=14 rho=-0.95   vol=.006776 u=323 $ Fat (BT)
41476-        324 like 1 but mat=5  rho=-1.009  vol=.006776 u=324 $ Eye (BT)
41477-        325 like 1 but mat=6  rho=-1.07   vol=.006776 u=325 $ TUMOR
41478-        326 like 1 but mat=6  rho=-1.07   vol=.006776 u=326 $ TUMOR
41479-        327 like 1 but mat=6  rho=-1.07   vol=.006776 u=327 $ TUMOR
41480-        328 like 1 but mat=6  rho=-1.07   vol=.006776 u=328 $ TUMOR
41481-        329 like 1 but mat=6  rho=-1.07   vol=.006776 u=329 $ TUMOR
41482-        330 like 1 but mat=6  rho=-1.07   vol=.006776 u=330 $ TUMOR
41483-        331 like 1 but mat=6  rho=-1.07   vol=.006776 u=331 $ TUMOR
```

```
41484-        332 like 1 but mat=6  rho=-1.07   vol=.006776 u=332 $ TUMOR
41485-        333 like 1 but mat=6  rho=-1.07   vol=.006776 u=333 $ TUMOR
41486-        334 like 1 but mat=6  rho=-1.07   vol=.006776 u=334 $ TUMOR
41487-        335 like 1 but mat=6  rho=-1.07   vol=.006776 u=335 $ TUMOR
41488-        336 like 1 but mat=6  rho=-1.07   vol=.006776 u=336 $ TUMOR
41489-        337 like 1 but mat=5  rho=-1.009  vol=.006776 u=337 $ Eye (BT)
41490-        338 like 1 but mat=5  rho=-1.009  vol=.006776 u=338 $ Eye (BT)
41491-        339 like 1 but mat=5  rho=-1.009  vol=.006776 u=339 $ Eye (BT)
41492-        340 like 1 but mat=5  rho=-1.009  vol=.006776 u=340 $ Eye (BT)
41493-        341 like 1 but mat=5  rho=-1.009  vol=.006776 u=341 $ Eye (BT)
41494-        342 like 1 but mat=5  rho=-1.009  vol=.006776 u=342 $ Eye (BT)
41495-        343 like 1 but mat=5  rho=-1.076  vol=.006776 u=343 $ Eye Ball (LT)
41496-        344 like 1 but mat=6  rho=-1.07   vol=.006776 u=344 $ TUMOR
41497-        345 like 1 but mat=6  rho=-1.07   vol=.006776 u=345 $ TUMOR
41498-        346 like 1 but mat=6  rho=-1.07   vol=.006776 u=346 $ TUMOR
41499-        347 like 1 but mat=5  rho=-1.009  vol=.006776 u=347 $ Eye (RT)
41500-        348 like 1 but mat=5  rho=-1.076  vol=.006776 u=348 $ Eye Ball (LT)
41501-        349 like 1 but mat=5  rho=-1.009  vol=.006776 u=349 $ Eye (RT)
41502-        350 like 1 but mat=5  rho=-1.076  vol=.006776 u=350 $ Eye Ball (LT)
41503-        351 like 1 but mat=5  rho=-1.009  vol=.006776 u=351 $ Eye (RT)
41504-        352 like 1 but mat=5  rho=-1.076  vol=.006776 u=352 $ Eye Ball (LT)
41505-        353 like 1 but mat=5  rho=-1.009  vol=.006776 u=353 $ Eye (RT)
41506-        354 like 1 but mat=5  rho=-1.009  vol=.006776 u=354 $ Eye (LT)
41507-        355 like 1 but mat=5  rho=-1.009  vol=.006776 u=355 $ Eye (RT)
41508-        356 like 1 but mat=14 rho=-0.95   vol=.006776 u=356 $ Fat (LT)
41509-        357 like 1 but mat=5  rho=-1.009  vol=.006776 u=357 $ Eye (RT)
41510-        358 like 1 but mat=14 rho=-0.95   vol=.006776 u=358 $ Fat (LT)
41511-        359 like 1 but mat=5  rho=-1.009  vol=.006776 u=359 $ Eye (RT)
41512-        360 like 1 but mat=14 rho=-0.95   vol=.006776 u=360 $ Fat (BT)
41513-        361 like 1 but mat=2  rho=-1.039  vol=.006776 u=361 $ Optic Nerve (BT)
41514-        362 like 1 but mat=14 rho=-0.95   vol=.006776 u=362 $ Fat (BT)
41515-        363 like 1 but mat=14 rho=-0.95   vol=.006776 u=363 $ Fat (BT)
41516-        364 like 1 but mat=14 rho=-0.95   vol=.006776 u=364 $ Fat (BT)
41517-        365 like 1 but mat=5  rho=-1.009  vol=.006776 u=365 $ Eye (LT)
41518-        366 like 1 but mat=6  rho=-1.07   vol=.006776 u=366 $ TUMOR
41519-        367 like 1 but mat=6  rho=-1.07   vol=.006776 u=367 $ TUMOR
41520-        368 like 1 but mat=6  rho=-1.07   vol=.006776 u=368 $ TUMOR
41521-        369 like 1 but mat=5  rho=-1.009  vol=.006776 u=369 $ Eye (RT)
41522-        370 like 1 but mat=5  rho=-1.009  vol=.006776 u=370 $ Eye (LT)
41523-        371 like 1 but mat=6  rho=-1.07   vol=.006776 u=371 $ TUMOR
41524-        372 like 1 but mat=6  rho=-1.07   vol=.006776 u=372 $ TUMOR
41525-        373 like 1 but mat=6  rho=-1.07   vol=.006776 u=373 $ TUMOR
41526-        374 like 1 but mat=5  rho=-1.009  vol=.006776 u=374 $ Eye (RT)
41527-        375 like 1 but mat=5  rho=-1.009  vol=.006776 u=375 $ Eye (LT)
41528-        376 like 1 but mat=6  rho=-1.07   vol=.006776 u=376 $ TUMOR
41529-        377 like 1 but mat=6  rho=-1.07   vol=.006776 u=377 $ TUMOR
41530-        378 like 1 but mat=6  rho=-1.07   vol=.006776 u=378 $ TUMOR
```

```
41531-        379 like 1 but mat=5  rho=-1.009  vol=.006776 u=379 $ Eye (RT)
41532-        380 like 1 but mat=5  rho=-1.009  vol=.006776 u=380 $ Eye (LT)
41533-        381 like 1 but mat=6  rho=-1.07   vol=.006776 u=381 $ TUMOR
41534-        382 like 1 but mat=6  rho=-1.07   vol=.006776 u=382 $ TUMOR
41535-        383 like 1 but mat=6  rho=-1.07   vol=.006776 u=383 $ TUMOR
41536-        384 like 1 but mat=5  rho=-1.009  vol=.006776 u=384 $ Eye (RT)
41537-        385 like 1 but mat=5  rho=-1.009  vol=.006776 u=385 $ Eye (FT)
41538-        386 like 1 but mat=6  rho=-1.07   vol=.006776 u=386 $ TUMOR
41539-        387 like 1 but mat=6  rho=-1.07   vol=.006776 u=387 $ TUMOR
41540-        388 like 1 but mat=6  rho=-1.07   vol=.006776 u=388 $ TUMOR
41541-        389 like 1 but mat=5  rho=-1.009  vol=.006776 u=389 $ Eye (FT)
41542-        390 like 1 but mat=5  rho=-1.009  vol=.006776 u=390 $ Eye (FT)
41543-        391 like 1 but mat=6  rho=-1.07   vol=.006776 u=391 $ TUMOR
41544-        392 like 1 but mat=6  rho=-1.07   vol=.006776 u=392 $ TUMOR
41545-        393 like 1 but mat=6  rho=-1.07   vol=.006776 u=393 $ TUMOR
41546-        394 like 1 but mat=5  rho=-1.009  vol=.006776 u=394 $ Eye (FT)
41547-        395 like 1 but mat=5  rho=-1.009  vol=.006776 u=395 $ Eye (FT)
41548-        396 like 1 but mat=6  rho=-1.07   vol=.006776 u=396 $ TUMOR
41549-        397 like 1 but mat=6  rho=-1.07   vol=.006776 u=397 $ TUMOR
41550-        398 like 1 but mat=6  rho=-1.07   vol=.006776 u=398 $ TUMOR
41551-        399 like 1 but mat=5  rho=-1.009  vol=.006776 u=399 $ Eye (FT)
41552-        400 like 1 but mat=5  rho=-1.009  vol=.006776 u=400 $ Eye (FT)
41553-        401 like 1 but mat=6  rho=-1.07   vol=.006776 u=401 $ TUMOR
41554-        402 like 1 but mat=6  rho=-1.07   vol=.006776 u=402 $ TUMOR
41555-        403 like 1 but mat=6  rho=-1.07   vol=.006776 u=403 $ TUMOR
41556-        404 like 1 but mat=5  rho=-1.009  vol=.006776 u=404 $ Eye (FT)
41557-        410 like 1 but mat=6  rho=-1.07   vol=.006776 u=410 $ Lens
41558-        411 like 1 but mat=6  rho=-1.07   vol=.006776 u=411 $ Lens
41559-        412 like 1 but mat=6  rho=-1.07   vol=.006776 u=412 $ Lens
41560-        413 like 1 but mat=6  rho=-1.07   vol=.006776 u=413 $ Lens
41561-        414 like 1 but mat=6  rho=-1.07   vol=.006776 u=414 $ Lens
41562-        415 like 1 but mat=6  rho=-1.07   vol=.006776 u=415 $ Lens
41563-        416 like 1 but mat=6  rho=-1.07   vol=.006776 u=416 $ Lens
41564-        417 like 1 but mat=6  rho=-1.07   vol=.006776 u=417 $ Lens
41565-        418 like 1 but mat=6  rho=-1.07   vol=.006776 u=418 $ Lens
41566-        419 like 1 but mat=6  rho=-1.07   vol=.006776 u=419 $ Lens
41567-        420 like 1 but mat=6  rho=-1.07   vol=.006776 u=420 $ Lens
41568-        421 like 1 but mat=6  rho=-1.07   vol=.006776 u=421 $ Lens
41569-        422 like 1 but mat=6  rho=-1.07   vol=.006776 u=422 $ Lens
41570-        423 like 1 but mat=6  rho=-1.07   vol=.006776 u=423 $ Lens
41571-        424 like 1 but mat=6  rho=-1.07   vol=.006776 u=424 $ Lens
41572-        425 like 1 but mat=6  rho=-1.07   vol=.006776 u=425 $ Lens
41573-        426 like 1 but mat=6  rho=-1.07   vol=.006776 u=426 $ Lens
41574-        427 like 1 but mat=6  rho=-1.07   vol=.006776 u=427 $ Lens
41575-        428 like 1 but mat=6  rho=-1.07   vol=.006776 u=428 $ Lens
41576-        429 like 1 but mat=6  rho=-1.07   vol=.006776 u=429 $ Lens
41577-        430 like 1 but mat=6  rho=-1.07   vol=.006776 u=430 $ Lens
```

```
41578-         431 like 1 but mat=6  rho=-1.07   vol=.006776 u=431 $ Lens
41579-         432 like 1 but mat=6  rho=-1.07   vol=.006776 u=432 $ Lens
41580-         433 like 1 but mat=6  rho=-1.07   vol=.006776 u=433 $ Lens
41581-         434 like 1 but mat=6  rho=-1.07   vol=.006776 u=434 $ Lens
41582-         435 like 1 but mat=6  rho=-1.07   vol=.006776 u=435 $ Lens
41583-         436 like 1 but mat=6  rho=-1.07   vol=.006776 u=436 $ Lens
41584-         437 like 1 but mat=6  rho=-1.07   vol=.006776 u=437 $ Lens
41585-         438 like 1 but mat=6  rho=-1.07   vol=.006776 u=438 $ Lens
41586-         439 like 1 but mat=6  rho=-1.07   vol=.006776 u=439 $ Lens
41587-         440 like 1 but mat=6  rho=-1.07   vol=.006776 u=440 $ Lens
41588-         441 like 1 but mat=6  rho=-1.07   vol=.006776 u=441 $ Lens
41589-         442 like 1 but mat=6  rho=-1.07   vol=.006776 u=442 $ Lens
41590-         443 like 1 but mat=6  rho=-1.07   vol=.006776 u=443 $ Lens
41591-         444 like 1 but mat=6  rho=-1.07   vol=.006776 u=444 $ Lens
41592-         445 like 1 but mat=6  rho=-1.07   vol=.006776 u=445 $ Lens
41593-         446 like 1 but mat=6  rho=-1.07   vol=.006776 u=446 $ Lens
41594-         447 like 1 but mat=6  rho=-1.07   vol=.006776 u=447 $ Lens
41595-         448 like 1 but mat=6  rho=-1.07   vol=.006776 u=448 $ Lens
41596-         449 like 1 but mat=6  rho=-1.07   vol=.006776 u=449 $ Lens
41597-         450 like 1 but mat=5  rho=-1.076  vol=.006776 u=450 $ Eye Ball (FT)
41598-         451 like 1 but mat=5  rho=-1.076  vol=.006776 u=451 $ Eye Ball (FT)
41599-         452 like 1 but mat=5  rho=-1.076  vol=.006776 u=452 $ Eye Ball (FT)
41600-         453 like 1 but mat=5  rho=-1.076  vol=.006776 u=453 $ Eye Ball (FT)
41601-         454 like 1 but mat=5  rho=-1.076  vol=.006776 u=454 $ Eye Ball (FT)
41602-         455 like 1 but mat=1  rho=-1 vol=.006776 u=455 $ water (FT/outside phantom)
41603-         456 like 1 but mat=1  rho=-1 vol=.006776 u=456 $ water (FT/outside phantom)
41604-         457 like 1 but mat=5  rho=-1.076  vol=.006776 u=457 $ Eye Ball (FT)
41605-         458 like 1 but mat=5  rho=-1.076  vol=.006776 u=458 $ Eye Ball (FT)
41606-         459 like 1 but mat=5  rho=-1.076  vol=.006776 u=459 $ Eye Ball (FT)
41607-         460 like 1 but mat=1  rho=-1 vol=.006776 u=460 $ water (FT/outside phantom)
41608-         461 like 1 but mat=1  rho=-1 vol=.006776 u=461 $ water (FT/outside phantom)
41609-         462 like 1 but mat=1  rho=-1 vol=.006776 u=462 $ water (FT/outside phantom)
41610-         463 like 1 but mat=1  rho=-1 vol=.006776 u=463 $ water (FT/outside phantom)
41611-         464 like 1 but mat=1  rho=-1 vol=.006776 u=464 $ water (FT/outside phantom)
41612-         465 like 1 but mat=5  rho=-1.076  vol=.006776 u=465 $ Eye Ball (FT)
41613-         466 like 1 but mat=5  rho=-1.076  vol=.006776 u=466 $ Eye Ball (FT)
41614-         467 like 1 but mat=5  rho=-1.076  vol=.006776 u=467 $ Eye Ball (FT)
41615-         468 like 1 but mat=5  rho=-1.076  vol=.006776 u=468 $ Eye Ball (FT)
41616-         469 like 1 but mat=5  rho=-1.076  vol=.006776 u=469 $ Eye Ball (FT)
41617-         470 like 1 but mat=1  rho=-1 vol=.006776 u=470 $ water (FT/outside phantom)
41618-         471 like 1 but mat=5  rho=-1.076  vol=.006776 u=471 $ Eye Ball (FT)
41619-         472 like 1 but mat=5  rho=-1.076  vol=.006776 u=472 $ Eye Ball (FT)
41620-         473 like 1 but mat=5  rho=-1.076  vol=.006776 u=473 $ Eye Ball (FT)
41621-         474 like 1 but mat=5  rho=-1.076  vol=.006776 u=474 $ Eye Ball (FT)
41622-         475 like 1 but mat=1  rho=-1 vol=.006776 u=475 $ water (FT/outside phantom)
41623-         476 like 1 but mat=1  rho=-1 vol=.006776 u=476 $ water (FT/outside phantom)
41624-         477 like 1 but mat=1  rho=-1 vol=.006776 u=477 $ water (FT/outside phantom)
```

```
41625-         478 like 1 but mat=1  rho=-1 vol=.006776 u=478 $ water (FT/outside phantom)
41626-         479 like 1 but mat=1  rho=-1 vol=.006776 u=479 $ water (FT/outside phantom)
41627-         480 like 1 but mat=5  rho=-1.076  vol=.006776 u=480 $ Eye Ball (FT)
41628-         481 like 1 but mat=5  rho=-1.076  vol=.006776 u=481 $ Eye Ball (FT)
41629-         482 like 1 but mat=5  rho=-1.076  vol=.006776 u=482 $ Eye Ball (FT)
41630-         483 like 1 but mat=5  rho=-1.076  vol=.006776 u=483 $ Eye Ball (FT)
41631-         484 like 1 but mat=5  rho=-1.076  vol=.006776 u=484 $ Eye Ball (FT)
41632-         485 like 1 but mat=1  rho=-1 vol=.006776 u=485 $ water (FT/outside phantom)
41633-         486 like 1 but mat=1  rho=-1 vol=.006776 u=486 $ water (FT/outside phantom)
41634-         487 like 1 but mat=5  rho=-1.076  vol=.006776 u=487 $ Eye Ball (FT)
41635-         488 like 1 but mat=5  rho=-1.076  vol=.006776 u=488 $ Eye Ball (FT)
41636-         489 like 1 but mat=5  rho=-1.076  vol=.006776 u=489 $ Eye Ball (FT)
41637-         490 like 1 but mat=1  rho=-1 vol=.006776 u=490 $ water (FT/outside phantom)
41638-         491 like 1 but mat=1  rho=-1 vol=.006776 u=491 $ water (FT/outside phantom)
41639-         492 like 1 but mat=1  rho=-1 vol=.006776 u=492 $ water (FT/outside phantom)
41640-         493 like 1 but mat=1  rho=-1 vol=.006776 u=493 $ water (FT/outside phantom)
41641-         494 like 1 but mat=1  rho=-1 vol=.006776 u=494 $ water (FT/outside phantom)
41642-         495 like 1 but mat=5  rho=-1.076  vol=.006776 u=495 $ Eye Ball (FT)
41643-         496 like 1 but mat=5  rho=-1.076  vol=.006776 u=496 $ Eye Ball (FT)
41644-         497 like 1 but mat=5  rho=-1.076  vol=.006776 u=497 $ Eye Ball (FT)
41645-         498 like 1 but mat=5  rho=-1.076  vol=.006776 u=498 $ Eye Ball (FT)
41646-         499 like 1 but mat=5  rho=-1.076  vol=.006776 u=499 $ Eye Ball (FT)
41647-         500 like 1 but mat=5  rho=-1.076  vol=.006776 u=500 $ Eye Ball (FT)
41648-         501 like 1 but mat=5  rho=-1.076  vol=.006776 u=501 $ Eye Ball (FT)
41649-         502 like 1 but mat=5  rho=-1.076  vol=.006776 u=502 $ Eye Ball (FT)
41650-         503 like 1 but mat=5  rho=-1.076  vol=.006776 u=503 $ Eye Ball (FT)
41651-         504 like 1 but mat=5  rho=-1.076  vol=.006776 u=504 $ Eye Ball (FT)
41652-         505 like 1 but mat=1  rho=-1 vol=.006776 u=505 $ water (FT/outside phantom)
41653-         506 like 1 but mat=1  rho=-1 vol=.006776 u=506 $ water (FT/outside phantom)
41654-         507 like 1 but mat=1  rho=-1 vol=.006776 u=507 $ water (FT/outside phantom)
41655-         508 like 1 but mat=1  rho=-1 vol=.006776 u=508 $ water (FT/outside phantom)
41656-         509 like 1 but mat=1  rho=-1 vol=.006776 u=509 $ water (FT/outside phantom)
41657-         515  0    99
41658-       c FT = Directly In Front of Tumor
41659-       c LT = Directly Left of Tumor
41660-       c RT = Directly Right of Tumor
41661-       c BT = Directly Behind Tumor
41662-
41663-           1 px  -8.91
41664-           2 px   9.79
41665-           3 py -13.42
41666-           4 py  10.56
41667-           5 pz  77.2
41668-           6 pz  94.
41669-           7 px   0
41670-           8 px    .22
41671-           9 py   0
```

```
41672-          10 py    .22
41673-          11 pz   0
41674-          12 pz    .14
41675-          38 c/z  0 3.41 .43
41676-          39 pz  70
41677-          40 c/z  0 3.41 .77
41678-          41 sq    .21236382 .35856431 0 0 0 0 -1 0 3.41 0
41679-          46 py  -4.05
41680-          49 sq    .024414062 .033667199 0 0 0 0 -1 0 -4.05 0
41681-          50 sq    .08650519  .067115895 0 0 0 0 -1 0 -4.05 0
41682-          51 pz  75.5
41683-          52 sq    .056689342 .016436554 0 0 0 0 -1 0 0 0
41684-          54 sq    .14792899 .147928994 .035599857 0 0 0 -1 0 -1.09 71.25
41685-          55 c/z  0 -1.09 1
41686-          56 sq    .21633315 .30864198 0 0 0 0 -1 0 -1.09 0
41687-          57 px   -.625
41688-          58 px    .625
41689-          59 py  -1.09
41690-          60 pz  70.5
41691-          61 pz  70.625
41692-          62 pz  71.875
41693-          63 pz  72.5
41694-          64 pz  75
41695-          65 sq    .016692372 .010412328 0 0 0 0 -1 0 0 0
41696-          66 py   4.8
41697-          67 pz  75.2
41698-          68 sq    .016692372 .010412328 -.00058209282 0 0 0 0 0 0 45.551971
41699-          70 c/z  0 1.2 5.81
41700-          72 sq    .015862038 .01 0 0 0 0 -1 0 0 0
41701-          73 py   5
41702-          74 c/z  0 1.2 6.01
41703-          75 sq    .015862038 .01 -.00058209282 0 0 0 0 0 0 45.551971
41704-          79 sq    .0025 .01 0 0 0 0 -1 0 0 0
41705-          81 sq    .0024507401 .0096116878 0 0 0 0 -1 0 0 0
41706-          99 sz  47 100
41707-         100 pz  94.5834
41708-
41709-       mode h p n e
 warning.  photonuclear physics may be needed (phys:p).
41710-       imp:h 1 383r 0
41711-       imp:p 1 383r 0
41712-       imp:n 1 383r 0
41713-       imp:e 1 383r 0
41714-       c Direct irradiation of the tumor w/ beam close to surface (Ideal Case)
41715-       c Source location (-2.42 -10.34 83.78) aimed in the y-direction into the tumor
41716-       sdef pos -2.42 -10.34 83.78 erg d2 vec 0 1 0 dir 1 ext 0 rad d1
 warning.  ext is constant.  in most problems it is a variable.
```

```
41717-              par h
41718-       phys:h 70
41719-       si1 0 .55
41720-       sp1 -21 1
41721-       si2 0 40.5802 40.7966 44.1944 47.5249 50.6795 53.6850 56.5626 59.3297 62
41722-       c
41723-       sp2 0 0.0509 .0020 0.0587 0.0665 0.0983 0.0902 0.1434 0.2220 0.47
41724-       c Water out side phantom [Oertli, 2006]
41725-       m1  1001 -0.11111 8016 -0.8889 hlib=.24h  $ Water
41726-       c Brain, grey matter, Optic Nerve [Duck FA, 1990]
41727-       m2  1001 -.107  6000 -.095  7014 -.018  8016 -.767
41728-             11023 -.002 15031 -.003 16000 -.002 17000 -.003
41729-             19000 -.003 hlib=.24h
41730-       c Brain, white matter [Duck FA, 1990]
41731-       m3  1001 -.106  6000 -.194  7014 -.025  8016 -.661
41732-             11023 -.002 15031 -.004 16000 -.002 17000 -.003
41733-             19000 -.003 hlib=.24h
41734-       c Cerebrospinal fluid [Duck FA, 1990]
41735-       m4  1001 -.111  8016 -.880 11023 -.005 17000 -.004 hlib=.24h
41736-       c Eyes [Duck FA, 1990]
41737-       m5  1001 -.107  6000 -.069  7014 -.017  8016 -.803
41738-             15031 -.001 16000 -.001 19000 -.002 hlib=.24h
41739-       c Eye lens, Adult [ICRU Report 46, 1992]
41740-       m6  1001 -.096  6000 -.195  7014 -.057  8016 -.646
41741-             11023 -.001 15031 -.001 16000 -.003 17000 -.001 hlib=.24h
41742-       c Muscle (skeletal), Adult [ICRU Report 46, 1992]
41743-       m7  1001 -.102  6000 -.143  7014 -.034  8016 -.710
41744-             11023 -.001 15031 -.002 16000 -.003 17000 -.001
41745-             19000 -.004 hlib=.24h
41746-       c Skeleton-cranium (whole), Adult [ICRU Report 46, 1992]
41747-       m8  1001 -.050  6000 -.212  7014 -.040  8016 -.435
41748-             11023 -.001 12000 -.002 15031 -.081 16000 -.003
41749-             20000 -.176 hlib=.24h
41750-       c Skeleton-cartilage, Adult [ICRU Report 46, 1992]
41751-       m9  1001 -.096  6000 -.099  7014 -.022  8016 -.744
41752-             11023 -.005 15031 -.022 16000 -.009 17000 -.003 hlib=.24h
41753-       c Skeleton-spongiosa, Adult [ICRU Report 46, 1992]
41754-       m10  1001 -.085  6000 -.404  7014 -.028  8016 -.367
41755-             11023 -.001 12000 -.001 15031 -.034 16000 -.002
41756-             17000 -.002 19000 -.001 20000 -.074 26056 -.001 hlib=.24h
41757-       c Spinal chord [Duck FA, 1990]
41758-       m11  1001 -.107  6000 -.145  7014 -.022  8016 -.712
41759-             11023 -.002 15031 -.004 16000 -.002 17000 -.003
41760-             19000 -.003 hlib=.24h
41761-       c Skin, Adult [ICRU Report 46, 1992]
41762-       m12  1001 -.100  6000 -.204  7014 -.042  8016 -.645
41763-             11023 -.002 15031 -.001 16000 -.002 17000 -.003
```

```
41764-            19000 -.001 hlib=.24h
41765-       c Thyroid, Adult [ICRU Report 46, 1992]
41766-       m13  1001 -.104  6000 -.119  7014 -.024  8016 -.745
41767-            11023 -.002 15031 -.001 16000 -.001 17000 -.002
41768-            19000 -.001 53127 -.001 hlib=.24h
41769-       c Adipose tissue, Adult #2 [ICRU Report 46, 1992]
41770-       m14  1001 -.114  6000 -.598  7014 -.007  8016 -.278
41771-            11023 -.001 16000 -.001 17000 -.001 hlib=.24h
41772-       F6:H 1 2 3 4 5 6 8 9 10 26 30 40 41 42 43 44 45 46 48
41773-            49 50 51 52 55 56 57 58 59 60 61 63 64 72 73 74
41774-            75 76 77 80 81 82 83 84 85 86 87 88 89 90 91 92
41775-            93 94 95 96 97 98 99 205 206 207 208 209 210 211
41776-            212 213 214 215 216 217 218 219 220 221 222 223
41777-            224 225 226 227 228 229 230 231 232 233 234 235
41778-            236 237 238 239 240 241 242 243 244 245 246 247
41779-            248 249 250 251 252 253 254 255 256 257 258 259
41780-            260 261 262 263 264 265 266 267 268 269 270 271
41781-            272 273 274 275 276 277 278 279 280 281 282 283
41782-            284 285 286 287 288 289 290 291 292 293 294 295
41783-            296 297 298 299 300 301 302 303 304 305 306 307
41784-            308 309 310 311 312 313 314 315 316 317 318 319
41785-            320 321 322 323 324 325 326 327 328 329 330 331
41786-            332 333 334 335 336 337 338 339 340 341 342 343
41787-            344 345 346 347 348 349 350 351 352 353 354 355
41788-            356 357 358 359 360 361 362 363 364 365 366 367
41789-            368 369 370 371 372 373 374 375 376 377 378 379
41790-            380 381 382 383 384 385 386 387 388 389 390 391
41791-            392 393 394 395 396 397 398 399 400 401 402 403
41792-            404 410 411 412 413 414 415 416 417 418 419 420
41793-            421 422 423 424 425 426 427 428 429 430 431 432
41794-            433 434 435 436 437 438 439 440 441 442 443 444
41795-            445 446 447 448 449 450 451 452 453 454 455 456
41796-            457 458 459 460 461 462 463 464 465 466 467 468
41797-            469 470 471 472 473 474 475 476 477 478 479 480
41798-            481 482 483 484 485 486 487 488 489 490 491 492
41799-            493 494 495 496 497 498 499 500 501 502 503 504
41800-            505 506 507 508 509
41801-       nps 300000
41802-       prdmp 2j 1
```

```
cell  1
                1.29645E-03 0.0106
cell  2
                1.24636E-06 0.7207
cell  3
                7.51061E-04 0.0187
cell  4
                2.23772E-06 0.2836
cell  5
                8.62917E-04 0.0143
cell  6
                0.00000E+00 0.0000
cell  8
                3.33380E-07 1.0000
cell  9
                0.00000E+00 0.0000
cell  10
                0.00000E+00 0.0000
cell  26
                0.00000E+00 0.0000
cell  30
                4.99060E-05 0.2235
cell  40
                0.00000E+00 0.0000
cell  41
                0.00000E+00 0.0000
cell  42
                0.00000E+00 0.0000
cell  43
                0.00000E+00 0.0000
cell  44
                0.00000E+00 0.0000
cell  45
                0.00000E+00 0.0000
cell  46
                3.06275E-01 0.0073
cell  48
                0.00000E+00 0.0000
cell  49
                0.00000E+00 0.0000
cell  50
                0.00000E+00 0.0000
cell  51
                0.00000E+00 0.0000
cell  52
                0.00000E+00 0.0000
cell  55
                0.00000E+00 0.0000
cell  56
                0.00000E+00 0.0000
cell  57
                0.00000E+00 0.0000
cell  58
                9.48006E-01 0.0065
cell  59
                0.00000E+00 0.0000
cell  60
                0.00000E+00 0.0000
cell  61
                0.00000E+00 0.0000
cell  63
                0.00000E+00 0.0000
cell  64
                0.00000E+00 0.0000
cell  72
                0.00000E+00 0.0000
cell  73
                0.00000E+00 0.0000
cell  74
                0.00000E+00 0.0000
cell  75
```

```
                0.00000E+00 0.0000
cell  76
                0.00000E+00 0.0000
cell  77
                0.00000E+00 0.0000
cell  80
                0.00000E+00 0.0000
cell  81
                0.00000E+00 0.0000
cell  82
                4.82408E-06 0.6117
cell  83
                0.00000E+00 0.0000
cell  84
                0.00000E+00 0.0000
cell  85
                0.00000E+00 0.0000
cell  86
                0.00000E+00 0.0000
cell  87
                0.00000E+00 0.0000
cell  88
                0.00000E+00 0.0000
cell  89
                0.00000E+00 0.0000
cell  90
                0.00000E+00 0.0000
cell  91
                0.00000E+00 0.0000
cell  92
                0.00000E+00 0.0000
cell  93
                0.00000E+00 0.0000
cell  94
                0.00000E+00 0.0000
cell  95
                4.59435E-05 0.3910
cell  96
                0.00000E+00 0.0000
cell  97
                0.00000E+00 0.0000
cell  98
                0.00000E+00 0.0000
cell  99
                4.96653E-03 0.1522
cell  205
                2.36855E+01 0.0184
cell  206
                3.40955E+01 0.0153
cell  207
                2.44975E+01 0.0183
cell  208
                2.41832E+01 0.0193
cell  209
                3.42971E+01 0.0160
cell  210
                2.50251E+01 0.0189
cell  211
                2.35561E+01 0.0206
cell  212
                3.48157E+01 0.0170
cell  213
                2.51087E+01 0.0201
cell  214
                2.21236E+01 0.0228
cell  215
                3.26843E+01 0.0187
cell  216
                2.32913E+01 0.0223
cell  217
                1.75603E+01 0.0269
```

```
cell  218
                2.40251E+01 0.0230
cell  219
                1.71710E+01 0.0272
cell  220
                9.23453E+00 0.0382
cell  221
                1.22857E+01 0.0328
cell  222
                9.20346E+00 0.0381
cell  223
                6.47344E+00 0.0345
cell  224
                2.33969E+01 0.0179
cell  225
                3.34152E+01 0.0148
cell  226
                2.36328E+01 0.0176
cell  227
                7.01634E+00 0.0337
cell  228
                6.63394E+00 0.0349
cell  229
                6.93939E+00 0.0345
cell  230
                7.05594E+00 0.0360
cell  231
                7.13998E+00 0.0358
cell  232
                7.34268E+00 0.0375
cell  233
                7.33679E+00 0.0369
cell  234
                7.11625E+00 0.0403
cell  235
                7.14643E+00 0.0402
cell  236
                6.39359E+00 0.0464
cell  237
                6.20197E+00 0.0455
cell  238
                3.27393E+00 0.0666
cell  239
                3.19878E+00 0.0651
cell  240
                7.18561E-01 0.1385
cell  241
                2.60561E+00 0.0721
cell  242
                3.55662E+00 0.0612
cell  243
                2.52651E+00 0.0715
cell  244
                6.25280E-01 0.1371
cell  245
                3.27520E+01 0.0155
cell  246
                5.42096E+01 0.0119
cell  247
                3.27724E+01 0.0157
cell  248
                3.34498E+01 0.0162
cell  249
                5.51431E+01 0.0125
cell  250
                3.25471E+01 0.0164
cell  251
                3.42287E+01 0.0172
cell  252
                5.59270E+01 0.0133
cell  253
```

```
                3.31940E+01 0.0174
cell  254
                3.18139E+01 0.0189
cell  255
                5.04778E+01 0.0149
cell  256
                3.14644E+01 0.0191
cell  257
                2.41594E+01 0.0229
cell  258
                3.78227E+01 0.0185
cell  259
                2.27377E+01 0.0237
cell  260
                1.22155E+01 0.0332
cell  261
                1.77545E+01 0.0270
cell  262
                1.19708E+01 0.0332
cell  263
                1.00846E+01 0.0273
cell  264
                3.17934E+01 0.0149
cell  265
                5.39829E+01 0.0115
cell  266
                3.25733E+01 0.0151
cell  267
                1.02634E+01 0.0275
cell  268
                1.03924E+01 0.0279
cell  269
                1.02527E+01 0.0283
cell  270
                1.07761E+01 0.0289
cell  271
                1.05987E+01 0.0290
cell  272
                1.09132E+01 0.0303
cell  273
                1.11014E+01 0.0304
cell  274
                1.05695E+01 0.0330
cell  275
                1.09777E+01 0.0330
cell  276
                8.61144E+00 0.0389
cell  277
                8.37846E+00 0.0393
cell  278
                4.34222E+00 0.0554
cell  279
                4.50599E+00 0.0554
cell  280
                8.40161E-01 0.1227
cell  281
                3.25248E+00 0.0626
cell  282
                5.43104E+00 0.0508
cell  283
                3.30140E+00 0.0633
cell  284
                9.86552E-01 0.1064
cell  285
                3.29342E+01 0.0154
cell  286
                5.38043E+01 0.0120
cell  287
                3.21972E+01 0.0156
cell  288
                3.39742E+01 0.0161
```

cell 289
5.32649E+01 0.0127
cell 290
3.30032E+01 0.0164
cell 291
3.42891E+01 0.0171
cell 292
5.41277E+01 0.0136
cell 293
3.40841E+01 0.0173
cell 294
3.22314E+01 0.0188
cell 295
4.84883E+01 0.0152
cell 296
3.11976E+01 0.0192
cell 297
2.34662E+01 0.0233
cell 298
3.61005E+01 0.0188
cell 299
2.30832E+01 0.0234
cell 300
1.19617E+01 0.0334
cell 301
1.69299E+01 0.0279
cell 302
1.18330E+01 0.0335
cell 303
1.03778E+01 0.0270
cell 304
3.27378E+01 0.0150
cell 305
5.41651E+01 0.0115
cell 306
3.22780E+01 0.0152
cell 307
1.03019E+01 0.0270
cell 308
1.05461E+01 0.0280
cell 309
1.07671E+01 0.0275
cell 310
1.06736E+01 0.0293
cell 311
1.09667E+01 0.0286
cell 312
1.11067E+01 0.0307
cell 313
1.12491E+01 0.0303
cell 314
1.05090E+01 0.0335
cell 315
1.07898E+01 0.0333
cell 316
8.54184E+00 0.0396
cell 317
7.99935E+00 0.0405
cell 318
4.46066E+00 0.0568
cell 319
3.75738E+00 0.0596
cell 320
1.02990E+00 0.1097
cell 321
3.55531E+00 0.0605
cell 322
5.07449E+00 0.0520
cell 323
3.59294E+00 0.0620
cell 324

```
                7.33969E-01 0.1324
cell  325
                2.50800E+01 0.0179
cell  326
                3.40759E+01 0.0154
cell  327
                2.41816E+01 0.0181
cell  328
                2.53067E+01 0.0188
cell  329
                3.48417E+01 0.0160
cell  330
                2.45005E+01 0.0190
cell  331
                2.50769E+01 0.0201
cell  332
                3.51502E+01 0.0170
cell  333
                2.47636E+01 0.0201
cell  334
                2.33593E+01 0.0223
cell  335
                3.16965E+01 0.0189
cell  336
                2.34587E+01 0.0222
cell  337
                1.77181E+01 0.0270
cell  338
                2.44109E+01 0.0229
cell  339
                1.76954E+01 0.0269
cell  340
                9.25840E+00 0.0384
cell  341
                1.22231E+01 0.0330
cell  342
                9.45103E+00 0.0378
cell  343
                6.23907E+00 0.0346
cell  344
                2.46930E+01 0.0174
cell  345
                3.39569E+01 0.0149
cell  346
                2.39116E+01 0.0177
cell  347
                6.63816E+00 0.0347
cell  348
                6.65942E+00 0.0352
cell  349
                6.67057E+00 0.0352
cell  350
                6.97738E+00 0.0364
cell  351
                6.87598E+00 0.0359
cell  352
                6.83314E+00 0.0383
cell  353
                7.25637E+00 0.0375
cell  354
                7.15437E+00 0.0415
cell  355
                7.27292E+00 0.0398
cell  356
                5.41892E+00 0.0505
cell  357
                5.90058E+00 0.0468
cell  358
                2.68538E+00 0.0725
cell  359
                3.29337E+00 0.0644
```

```
cell  360
                5.57763E-01 0.1530
cell  361
                2.16068E+00 0.0756
cell  362
                3.78887E+00 0.0609
cell  363
                2.38700E+00 0.0744
cell  364
                6.28935E-01 0.1399
cell  365
                6.36436E+00 0.0336
cell  366
                2.26233E+01 0.0174
cell  367
                3.22583E+01 0.0145
cell  368
                2.28244E+01 0.0172
cell  369
                6.63097E+00 0.0325
cell  370
                9.72689E+00 0.0271
cell  371
                3.15448E+01 0.0147
cell  372
                5.30822E+01 0.0111
cell  373
                3.17452E+01 0.0148
cell  374
                9.72936E+00 0.0270
cell  375
                9.84195E+00 0.0268
cell  376
                3.15995E+01 0.0146
cell  377
                5.29154E+01 0.0111
cell  378
                3.12213E+01 0.0149
cell  379
                1.00279E+01 0.0265
cell  380
                6.01238E+00 0.0342
cell  381
                2.41752E+01 0.0170
cell  382
                3.24157E+01 0.0145
cell  383
                2.33933E+01 0.0171
cell  384
                6.30462E+00 0.0335
cell  385
                5.75280E+00 0.0332
cell  386
                2.16833E+01 0.0168
cell  387
                3.05437E+01 0.0143
cell  388
                2.18598E+01 0.0169
cell  389
                6.08106E+00 0.0326
cell  390
                8.97319E+00 0.0267
cell  391
                2.97788E+01 0.0143
cell  392
                5.02842E+01 0.0109
cell  393
                2.95769E+01 0.0144
cell  394
                9.20284E+00 0.0264
cell  395
```

```
                9.09944E+00 0.0266
cell  396
                2.94742E+01 0.0143
cell  397
                5.05707E+01 0.0108
cell  398
                2.94877E+01 0.0145
cell  399
                9.17632E+00 0.0259
cell  400
                5.64607E+00 0.0336
cell  401
                2.26957E+01 0.0164
cell  402
                3.00947E+01 0.0141
cell  403
                2.20488E+01 0.0167
cell  404
                5.95038E+00 0.0331
cell  410
                0.00000E+00 0.0000
cell  411
                4.64009E-02 0.3810
cell  412
                3.20366E-04 1.0000
cell  413
                8.32163E-03 1.0000
cell  414
                0.00000E+00 0.0000
cell  415
                0.00000E+00 0.0000
cell  416
                0.00000E+00 0.0000
cell  417
                5.77752E-03 1.0000
cell  418
                1.00388E-02 0.8959
cell  419
                0.00000E+00 0.0000
cell  420
                7.86376E-02 0.3325
cell  421
                1.47088E-02 0.4703
cell  422
                3.06120E-03 1.0000
cell  423
                1.23589E-02 1.0000
cell  424
                4.18576E-02 0.5223
cell  425
                9.02344E-03 0.7383
cell  426
                9.91177E-03 1.0000
cell  427
                4.18945E-03 0.8838
cell  428
                5.27046E-03 1.0000
cell  429
                0.00000E+00 0.0000
cell  430
                4.28151E-02 0.4049
cell  431
                1.39836E-02 0.5984
cell  432
                0.00000E+00 0.0000
cell  433
                0.00000E+00 0.0000
cell  434
                2.07339E-02 0.9231
cell  435
                3.31669E-02 0.6738
```

```
cell  436
                5.46662E-02 0.4044
cell  437
                1.87302E-02 0.5569
cell  438
                0.00000E+00 0.0000
cell  439
                0.00000E+00 0.0000
cell  440
                1.79018E-02 0.7434
cell  441
                0.00000E+00 0.0000
cell  442
                0.00000E+00 0.0000
cell  443
                0.00000E+00 0.0000
cell  444
                0.00000E+00 0.0000
cell  445
                4.41266E-03 1.0000
cell  446
                0.00000E+00 0.0000
cell  447
                0.00000E+00 0.0000
cell  448
                0.00000E+00 0.0000
cell  449
                0.00000E+00 0.0000
cell  450
                5.18373E+00 0.0323
cell  451
                2.05223E+01 0.0166
cell  452
                2.84513E+01 0.0139
cell  453
                2.04410E+01 0.0164
cell  454
                5.52579E+00 0.0324
cell  455
                4.86820E+00 0.0322
cell  456
                1.89253E+01 0.0159
cell  457
                2.63090E+01 0.0137
cell  458
                1.91076E+01 0.0161
cell  459
                4.95625E+00 0.0314
cell  460
                4.58518E+00 0.0320
cell  461
                1.79874E+01 0.0158
cell  462
                2.51497E+01 0.0135
cell  463
                1.81455E+01 0.0159
cell  464
                4.67990E+00 0.0316
cell  465
                8.26304E+00 0.0267
cell  466
                2.78459E+01 0.0139
cell  467
                4.71650E+01 0.0105
cell  468
                2.75318E+01 0.0140
cell  469
                8.53846E+00 0.0255
cell  470
                7.67955E+00 0.0259
cell  471
```

```
                2.59392E+01 0.0137
cell  472
                4.37731E+01 0.0102
cell  473
                2.56451E+01 0.0137
cell  474
                7.83693E+00 0.0254
cell  475
                7.29560E+00 0.0255
cell  476
                2.47861E+01 0.0135
cell  477
                4.18187E+01 0.0102
cell  478
                2.43861E+01 0.0137
cell  479
                7.26601E+00 0.0250
cell  480
                8.28389E+00 0.0258
cell  481
                2.73929E+01 0.0139
cell  482
                4.68410E+01 0.0105
cell  483
                2.74736E+01 0.0140
cell  484
                8.51040E+00 0.0256
cell  485
                7.74127E+00 0.0255
cell  486
                2.58056E+01 0.0137
cell  487
                4.40292E+01 0.0103
cell  488
                2.57997E+01 0.0140
cell  489
                7.91637E+00 0.0250
cell  490
                7.41962E+00 0.0253
cell  491
                2.45890E+01 0.0135
cell  492
                4.21070E+01 0.0102
cell  493
                2.44373E+01 0.0137
cell  494
                7.68348E+00 0.0247
cell  495
                5.20738E+00 0.0327
cell  496
                2.13501E+01 0.0161
cell  497
                2.84401E+01 0.0138
cell  498
                2.05777E+01 0.0163
cell  499
                5.37283E+00 0.0319
cell  500
                4.88976E+00 0.0326
cell  501
                1.98033E+01 0.0157
cell  502
                2.63698E+01 0.0135
cell  503
                1.92335E+01 0.0161
cell  504
                4.87555E+00 0.0321
cell  505
                4.59496E+00 0.0321
cell  506
                1.88146E+01 0.0156
```

```
cell  507
                2.48636E+01 0.0134
cell  508
                1.83901E+01 0.0158
cell  509
                4.57277E+00 0.0323
```

1analysis of the results in the tally fluctuation chart bin (tfc) for tally   6 with nps =    300000    print table 160

 normed average tally per history  = 1.29645E-03          unnormed average tally per history  = 3.28072E-01
 estimated tally relative error    = 0.0106               estimated variance of the variance  = 0.0004
 relative error from zero tallies  = 0.0097               relative error from nonzero scores  = 0.0042

 number of nonzero history tallies =        9600          efficiency for the nonzero tallies  = 0.0960
 history number of largest  tally  =       75805          largest  unnormalized history tally = 2.33394E+01
 (largest  tally)/(average tally)  = 7.11412E+01          (largest  tally)/(avg nonzero tally)= 6.82955E+00

 (confidence interval shift)/mean  = 0.0001               shifted confidence interval center  = 1.29655E-03

 if the largest  history score sampled so far were to occur on the next history, the tfc bin quantities would change as follows:

| estimated quantities | value at nps | value at nps+1 | value(nps+1)/value(nps)-1. |
|---|---|---|---|
| mean | 1.29645E-03 | 1.29736E-03 | 0.000701 |
| relative error | 1.05859E-02 | 1.06016E-02 | 0.001480 |
| variance of the variance | 3.62682E-04 | 3.78499E-04 | 0.043612 |
| shifted center | 1.29655E-03 | 1.29655E-03 | 0.000001 |
| figure of merit | 2.49085E+03 | 2.48350E+03 | -0.002954 |

 the estimated slope of the 200 largest  tallies starting at  6.75804E+00 appears to be decreasing at least exponentially.
 the large score tail of the empirical history score probability density function appears to have no unsampled regions.

==========

          results of 10 statistical checks for the estimated answer for the tally fluctuation chart (tfc) bin of tally   6

| tfc bin | --mean-- | ---------relative error--------- | | | ----variance of the variance---- | | | --figure of merit-- | | -pdf- |
|---|---|---|---|---|---|---|---|---|---|---|
| behavior | behavior | value | decrease | decrease rate | value | decrease | decrease rate | value | behavior | slope |
| desired | random | <0.10 | yes | 1/sqrt(nps) | <0.10 | yes | 1/nps | constant | random | >3.00 |
| observed | random | 0.01 | yes | yes | 0.00 | yes | yes | constant | random | 10.00 |
| passed? | yes | yes | yes | yes | yes | yes | yes | yes | yes | yes |

 ==========

 this tally meets the statistical criteria used to form confidence intervals: check the tally fluctuation chart to verify.
 the results in other bins associated with this tally may not meet these statistical criteria.

 estimated asymmetric confidence interval(1,2,3 sigma): 1.2828E-03 to 1.3103E-03; 1.2691E-03 to 1.3240E-03; 1.2554E-03 to 1.3377E-03
 estimated  symmetric confidence interval(1,2,3 sigma): 1.2827E-03 to 1.3102E-03; 1.2690E-03 to 1.3239E-03; 1.2553E-03 to 1.3376E-03

 fom = (histories/minute)*(f(x) signal-to-noise ratio)**2 = (2.791E+04)*( 2.987E-01)**2 = (2.791E+04)*(8.924E-02) = 2.491E+03

```
1status of the statistical checks used to form confidence intervals for the mean for each tally bin

 tally   result of statistical checks for the tfc bin (the first check not passed is listed) and error magnitude check for all bins

     6   passed the 10 statistical checks for the tally fluctuation chart bin result
         missed all bin error check:   358 tally bins had    64 bins with zeros and    37 bins with relative errors exceeding 0.10

 the 10 statistical checks are only for the tally fluctuation chart bin and do not apply to other tally bins.

 the tally bins with zeros may or may not be correct: compare the source, cutoffs, multipliers, et cetera with the tally bins.

 warning.     1 of the   1 tallies had bins with relative errors greater than recommended.
1tally fluctuation charts

                      tally    6
      nps      mean     error   vov  slope    fom
     8000   1.2405E-03 0.0367 0.0034  3.5    2589
    16000   1.2958E-03 0.0259 0.0020  3.6    2571
    24000   1.2923E-03 0.0213 0.0013  3.6    2566
    32000   1.3060E-03 0.0184 0.0010  3.5    2580
    40000   1.3031E-03 0.0166 0.0008  3.5    2541
    48000   1.2952E-03 0.0152 0.0007  3.5    2523
    56000   1.2890E-03 0.0140 0.0005  4.4    2525
    64000   1.2959E-03 0.0131 0.0005  6.1    2512
    72000   1.3014E-03 0.0124 0.0005 10.0    2503
    80000   1.3001E-03 0.0118 0.0004 10.0    2488
    88000   1.3004E-03 0.0113 0.0004 10.0    2496
    96000   1.2982E-03 0.0108 0.0004 10.0    2481
   300000   1.2965E-03 0.0106 0.0004 10.0    2491

 ************************************************************************************************************************
 dump no.    2 on file runtpe       nps =      300000   coll =       46515183     ctm =    3.58     nrn =      275976506

 tally data written to file mctal

        16 warning messages so far.


 run terminated when    300000 particle histories were done.

 computer time =    4.88 minutes

 mcnpx    version 2.5.0 Mon Mar 21 08:00:00 MST 2005               04/07/07 19:54:32     probid =   04/07/07 19:49:22
```

# VITA


| | |
|---|---|
| Name: | Brian Edward Massingill |
| Address: | Department of Nuclear Engineering<br>Texas A&M University<br>3133 TAMU<br>College Station, TX 77843-3133 |
| Email Address: | bmassingill@gmail.com |
| Education: | B.S., Radiological Health Engineering, Texas A&M University, 2005<br>M.S., Health Physics, Texas A&M University, 2007 |